INSTITUTO TECNOLÓGICO Y DE ESTUDIOS SUPERIORES DE OCCIDENTE

Reconocimiento de validez oficial de estudios de nivel superior según acuerdo secretarial 15018, publicado en el Diario Oficial de la Federación el 29 de noviembre de 1976.

Departamento de Electrónica, Sistemas e Informática

MAESTRÍA EN DISEÑO ELECTRÓNICO

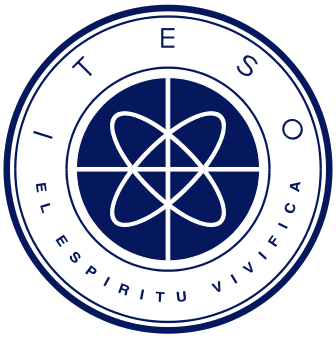

MODELADO DE INTERCONEXIONES SINGLE-ENDED EMPLEANDO TÉCNICAS DE MODELO SUSTITUTO Y DISEÑO DE EXPERIMENTOS

Tesis que para obtener el grado de

MAESTRA EN DISEÑO ELECTRÓNICO

Presenta: Aurea Edna Moreno Mojica

Director de tesis: Dr. Zabdiel Brito Brito

Tlaquepaque, Jalisco. Agosto de 2016.

MAESTRO EN INGENIERÍA (2016) ITESO

Maestría en Diseño Electrónico Tlaquepaque, Jal., México

TÍTULO: **Modelado De Interconexiones Single-Ended Empleando Técnicas de Modelo Sustituto y Diseño de Experimentos**

AUTOR: Aurea Edna Moreno Mojica
Ingeniero en Electrónica (ITESO, México)

DIRECTOR DE TESIS: Zabdiel Brito Brito
Departamento de Electrónica, Sistemas e Informática, ITESO
Ingeniero en Comunicaciones y Electrónica (IPN, México)
Maestro en Ingeniería Electrónica (IPN, México)
Doctor en Comunicaciones y Teoría de la Señal (Universidad Politécnica de Cataluña, España)

NÚMERO DE PÁGINAS: ix, 66

Resumen

En este trabajo se estudió una topología punto-a-punto, compuesta por un buffer maestro, su paquete, dos líneas de transmisión de longitudes L1 y L2 con una resistencia en serie en el PCB, y un buffer esclavo, donde la respuesta considerada para el sistema fue el tiempo de vuelo de las señales digitales provenientes de los buffers. Las simulaciones por lo general se realizaban utilizando un simulador SPICE modelando la topología en secciones. Para disminuir los recursos computacionales durante procesos de optimización, se obtuvieron modelos sustitutos utilizando el diseño de experimentos, ya que no existe un modelo analítico del sistema completo.

Para construir el modelo sustituto se realizaron experimentos de cribado. Tres factores no-controlables tuvieron un efecto significativo en el tiempo de vuelo de la señal del buffer maestro: la impedancia característica (Zo) de las líneas de transmisión del PCB y las condiciones de operación de los dos buffers. Estos factores también fueron significativos para la señal procedente del buffer esclavo, así como la Zo de las líneas de transmisión del paquete.

Se comparó el ajuste de diseños compuestos centrales rotables y "face-centered", considerando un error máximo de 15%. Los diseños "face-centered" fueron menos complejos y proporcionaron un mejor ajuste del modelo, sin embargo fueron menos poderosos en la extrapolación de las predicciones. Los diseños rotables estuvieron limitados en el intervalo permitido para las longitudes de L1 y L2.

Mediante los modelos sustitutos desarrollados para las interconexiones se representó un bus síncrono, el "Serial Peripheral Interface" (SPI), que requiere un análisis de tiempo para evaluar la longitud máxima permitida de las líneas de transmisión. Un algoritmo Nelder-Mead con función de penalización añadida se utilizó para optimizar las longitudes L1 y L2 del modelo sustituto, mantenimiento los márgenes de tiempo igual o mayores que cero. Las longitudes óptimas se validaron utilizando simulaciones SPICE.

Summary

A point-to-point topology was studied in this work, consisting of a master buffer, its package, two transmission lines of lengths L1 and L2 with a series resistor on the PCB, and a slave buffer. The considered response for the system was the flight time of digital signals coming out of the buffers. Simulations usually were done using a SPICE simulator by modelling the topology in sections. To decrease computational resources during optimization processes, surrogate models were obtained using design of experiments since no analytical model of the complete system exists.

In order to build the surrogate model, screening experiments were done. Three uncontrollable factors proved to have a significant effect on the flight time of the signal from the master buffer: the characteristic impedance (Zo) of the PCB transmission lines and the operating conditions of both buffers. These three factors were also significant for the signal coming from the slave buffer, in addition to the Zo of the package transmission lines.

Face-centered and rotatable central composite designs for both the master and slave signals were compared to see which had a better fit, with a 15% maximum error. The face-centered designs were less complex and provided a better model fit, however they were less powerful at extrapolating predictions. The rotatable designs were limited in the allowable range for the lengths of L1 and L2.

The surrogate models developed for the interconnects allowed to represent a Serial Peripheral Interface (SPI), which is a synchronous bus, and requires a timing analysis to assess the maximum allowed length of the transmission lines. A Nelder-Mead algorithm with an added penalty function was used to optimize the surrogate model lengths L1 and L2, while maintaining the timing margins equal to or larger than zero. Optimal lengths were validated using SPICE simulations.

Content

Summary ..... **vii**

Content ..... **ix**

Introduction **1**

1. Screening Experiment **3**

1.1. MODEL OF THE TOPOLGY 4
1.2. BASICS ON DESIGN OF EXPERIMENTS 7
1.3. DESIGN OF EXPERIMENTS FOR THE SELECTED TOPOLOGY 10
1.4. FLIGHT TIME MEASUREMENT 12
1.5. CONCLUSIONS 19

2. The Surrogate Model **21**

2.1. CONSTRUCTING THE MODEL 21
2.2. VALIDATING THE MODEL 37
2.3. APPLYING THE MODEL 43
2.4. CONCLUSIONS 48

3. Direct Optimization of SPI Interface Using Surrogate Models **49**

3.1. NELDER-MEAD ALGORITHM 49
3.2. IMPLEMENTING THE ALGORITHM 52
3.3. OPTIMIZATION RESULTS USING FMINSEARCH 54
3.4. CONCLUSIONS 58

Conclusions **59**

Future Work **61**

Bibliography **63**

Index **65**

Introduction

Design guidelines are developed for the interconnections of server platforms that support the latest generation of Intel processors and chipsets at the group "Enterprise Platform Signal Integrity" at Intel. Typically, these guidelines are made for differential and single-ended signals, the latter of which have a subset of interfaces that are considered low speed, and operate at a maximum frequency of 200MHz. These low speed signals serve several different purposes and can have different topologies for a single interface.

Today there is an inefficient design methodology for the guidelines for the single-ended low speed interconnections. The design process involves time domain simulations of specific cases, in which voltage levels are measured for some types of signals, or propagation time for others. A simulation file in SPICE format is written for each of the different existing topologies, and 32 cases are simulated per topology, corresponding to the combinations of five process variables (the most common being characteristic impedances and voltage levels). These variables are chosen without any study to see which variables have more effect on the system. The simulations are relatively fast, each case is simulated in less than 10 minutes (more complex topologies may have longer simulation times) however the analysis done for the simulations works only for the specific topology simulated. When a change in a variable is required, the 32 cases of the topology need to be simulated and analyzed again.

In this thesis, a methodology is defined to obtain surrogate model of single-ended low-speed interconnects for server platforms, that are useful in simplifying optimization tasks. The methodology involves selecting the variables with the greatest impact on the response of the system, and using mathematical modeling and design of experiments techniques to develop the surrogate models.

Surrogate modeling refers to the modelling of a complex system at less computational cost. Unlike the complex system, the “surrogate” should be easier to evaluate, whereby the accuracy and range of applicability are traded off. Sampling is an essential part of surrogate modeling, and includes two important modeling criteria. The first is the number of elements in the vectors, and the second is the range of the variables. The number of elements of the sample vectors can

substantially change the complexity of the final surrogate models [Yelten-12]. In the first chapter, an experimental design will be used for the selection of important variables to consider for the system studied. In Chapter 2 the range of the variables will be decided.

Surrogate modeling that aims to describe the whole possible ranges of the inputs is more computationally expensive to develop and use, and requires a large number of samples. This number can be optimized by using a well-defined sampling plan [Yelten-12]. In Chapter 2 different types of design of experiments will be considered to develop a mathematical model that accurately represents the behavior of the system from the chosen variables in Chapter 1, using the least possible samples.

Accuracy of the surrogate models should be carefully quantified as this what decides the usefulness of the models developed. Test vectors, different from the sample vectors, must be created that will be used to validate the surrogate models [Yelten-12]. In Chapter 2, the models obtained from the different types of experiments, are validated and the error between the response of actual system and the estimated response, is then quantified using the root mean square error (RMSE). Furthermore, the surrogate models obtained will be validated in the design space. Finally, in Chapter 3 the models obtained in Chapter 2 will be used in a practical application of optimization, and the optimized results will be validated in a SPICE simulation.

1. Screening Experiment

Interconnections of server platforms are made for differential and single-ended signals, the latter of which have a subset of low speed interfaces that serve for several different purposes and have different topologies. A simple point-to-point topology has been chosen to be studied in this work, consisting of a master device, the master's package, two transmission lines of lengths L1 and L2 with a series resistor on the printed circuit board (PCB), and a slave device. For this system, the response to be considered is the flight time of digital signals, which is the time that it takes the signal to go through all the components starting from one device all the way to the other. Fig. 1-1 shows the point-to-point topology as seen from the side view.

Manufacturing electronic circuit prototypes of any topology for its analysis would be costly and time consuming. CAD tools (circuit analysis programs assisted by computer) provide a simple and cost-effective electronic circuit simulation environment. By simulating the circuits, errors can be detected and different components can be explored. The simulation of an electronic system can also be helpful to deepen the knowledge of the behavior of the circuit.

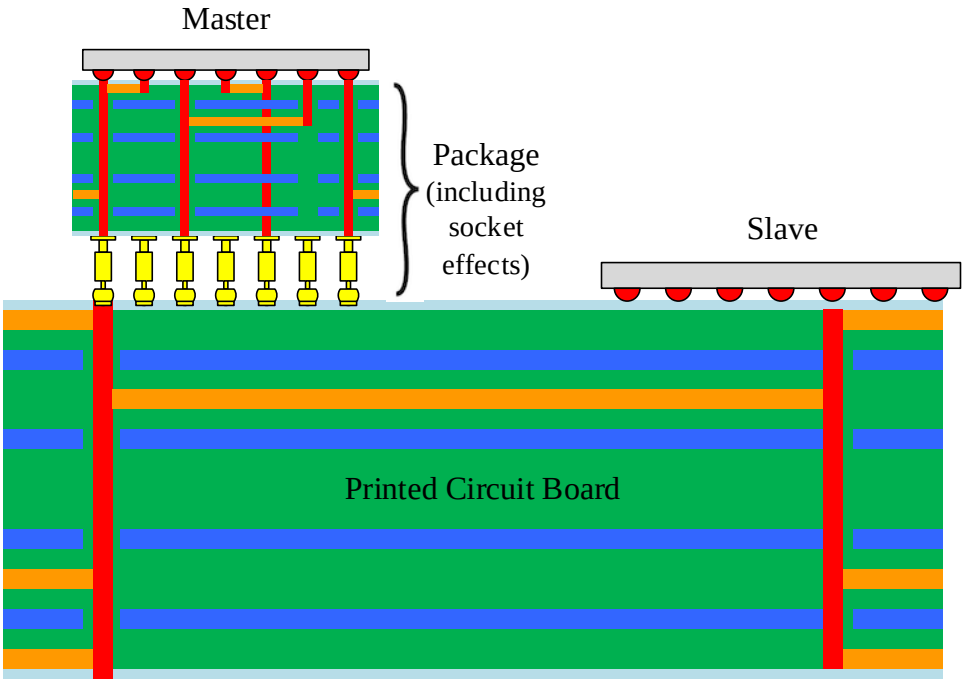

Fig. 1-1 Typical point-to-point topology seen from the side view showing the master and slave devices, master package, and printed circuit board.

1.1. Model of the Topolgy

Simulating the complete topology in Fig. 1-1 would require expensive 3D modelling and simulation. To decrease computational resources, the topology is divided into sections and modelled separately. Behavioral models are extracted for the R_{on} value of the pull-up and pull-down transistors of the buffers for both master and slave. 3D and 2D simulation is used to extract parameter values for distributed element models for the transmission lines of the package and the PCB. Lumped element models are used for the passive components such as resistors. Fig. 1-2 shows the simplified topology.

All the different simulation models that make up the system's topology are linked together in a simulation program. In electronics, the worldwide standard circuit simulator is called SPICE (Simulation Program with Integrated Circuit Emphasis). SPICE was developed at UC Berkley and was made available to the public in July 1975. SPICE was designed to determined unknown parameters using Kirchhoff current equations in nodal analysis. It is an all-purpose simulation program for non-linear DC analysis, non-linear transient analysis, and linear AC analysis. The simulated circuits can contain resistors, capacitors, inductors, magnetic coupling, current and voltage sources, transmission lines, switches, and semiconductor devices [Savant-98]. SPICE simulates the behavior of electronic circuits and tries to emulate signal generators, as well as measurement equipment like oscilloscopes, multimeters, curve tracers and frequency spectrum analyzers.

SPICE simulators provide the analysis of the electronic circuit's performance by using Monte Carlo analysis, parametric sweeps, as well as optimization methods. In order to perform a simulation the first thing to do is to generate a netlist, which is a textual representation of the electronic circuit with all components interconnected. Using models as the ones listed above for

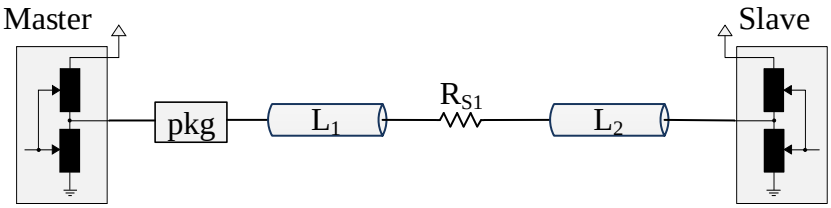

Fig. 1-2 Simplified point-to-point topology showing master and slave devices, master package, transmission lines of lengths L1 and L2, and a serial resistor.

each component, the netlist is then converted by the simulator into mathematical matrices that will be solved according to the specified type of analysis.

In the design process it is sometimes impractical to base the analysis on simulations of the electronic circuit. Each time a component's value needs to be changed, the entire simulation needs to be run again, and depending on the complexity of the circuit this can take up to hours. Many times new models need to be generated for each new simulation, adding time to the process. For these reasons, it is sometimes more convenient to do the analysis using surrogate models.

In general, a process or system can be represented by the model in Fig. 1-3, that consists of a combination of resources that transform an input into an output, which has one or more observable response variables. Some of the system's properties $x_1,x_2,\ldots,x_p$ are controllable, whereas other variables $z_1,z_2,\ldots,z_q$ are uncontrollable [Montgomery-13]. This model enables the system to be viewed as a black box that represents very closely the behavior of the original system within a determined range of its input variables. The idea of a substitute model is to use this alternative representation to analyze the system, without having to simulate the entirety of it again.

Systems like the one chosen in this work are subject to Process, Voltage, and Temperature (PVT) variations that have a direct effect on all the components in the circuit. For the system in Fig. 1-2 voltage and temperature have a direct effect on the impedance of the buffers modelling the master and slave. Temperature and process variations have a direct effect on the characteristic impedance (Zo) of the transmission lines in the circuit. Process variations directly affect the value

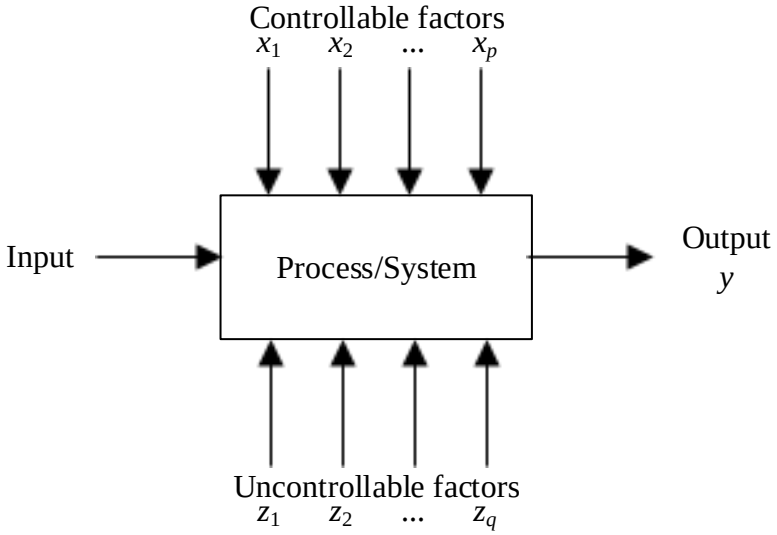

Fig. 1-3 General model of a process or system showing the output, the input, controllable and uncontrollable factors.

of the passive elements. These factors in practice are uncontrollable and are assumed to stay within an allowable range, or tolerance from the nominal value, and thus have a maximum and a minimum value (these values are called corners). The uncontrollable factors and their permissible range for the point-to-point topology discussed in this work are presented in TABLE I. For this work, the controllable factors chosen are the lengths of the transmission lines on the PCB. The length of the transmission lines in the package are not considered design factors as the lengths are fixed and cannot be changed.

The simulation models for the buffers used in this work use IBIS files containing behavioral and electrical characteristics of the input and output buffers. Models using IBIS files do not follow conventional modelling ideas as a schematic symbol or polynomial expression. An IBIS file consists of tabular data of current-voltage relationship values (which give the R_{on} value of the pull-up and pull-down transistors of the buffer), as well as the voltage-time relationship at the output pins under rising and falling switching conditions. The files are generated for three different corner conditions: nominal, minimum, and maximum. In a nominal condition, the data is obtained for nominal supply voltage and nominal temperature; in a minimum condition, the data is obtained with the minimum supply voltage, and maximum temperature; and for a maximum condition, maximum supply voltage and minimum temperature are used [Casamayor-04]. For this reason, a single simulation parameter is used to select operating conditions of the IBIS data, therefore the

TABLE I
UNCONTROLLABLE FACTORS FOR POINT-TO-POINT TOPOLOGY

Factor	Minimum	Nominal	Maximum
Voltage	3.135 V	3.3 V	3.465 V
Temperature	0 °C	50 °C	110 °C
Buffer pull-up impedance	20 ohm	25 ohm	30 ohm
Buffer pull-down impedance	15 ohm	20 ohm	25 ohm
Series resistor value	31.35 ohm	33 ohm	34.65 ohm
Zo of board routing	42.5 ohm	50 ohm	57.5 ohm
Zo of package routing	46 ohm	50 ohm	54 ohm

TABLE II
UNCONTROLLABLE FACTORS CHOSEN FOR SIMULATION

Factor	Minimum	Nominal	Maximum
master_corner	3.135 V, 110 °C and operating conditions at minimum value	3.30 V, 50 °C and operating conditions at typical value	3.465 V, 0 °C and operating conditions at maximum value
slave_corner	3.135 V, 110 °C and operating conditions at minimum value	3.30 V, 50 °C and operating conditions at typical value	3.465 V, 0 °C and operating conditions at maximum value
Series resistor value	31.35 ohm	33 ohm	34.65 ohm
Zo of board routing	42.5 ohm	50 ohm	57.5 ohm
Zo of package routing	46 ohm	50 ohm	54 ohm

factors in TABLE II are used in the simulation for this experiment, instead of the ones listed in TABLE I.

1.2. Basics on Design of Experiments

For complex systems like electronic circuits, there is usually no analytical model of the complete system. In such cases, design of experiments comes in handy. Experiments are used to study the performance of processes and systems, and well-designed experiments can lead to empirical models that can be manipulated as if they were analytical models [Montgomery-13].

In any system, some variables may have a larger influence over the system's response than others. This is why before submitting the system to an experiment that will hopefully result in a useful empirical model, the first step in experimental design is to run a screening experiment to see which factors are the most important and use only those in subsequent experiments. The most efficient way to screen the design factors is to conduct a factorial experiment. In this strategy, a complete trial of the experiment consists in all possible combinations of the levels of the factors

involved. The effect of a factor is the change in the response produced by a change in the level of the factor. The level of the factors is the number of values that are assigned to each factor in the experiment. When the effect of a factor depends on the level of another factor, it is said that an interaction exists between these factors [Montgomery-13].

The most common type of experimental designs used in screening experiments are factorial designs of only 2 levels, since "this type of design provides the smallest number of runs which *k* factors can be studied in a complete factorial design" [Montgomery-13]. The levels in these designs are usually called "low" and "high", and correspond to the minimum and maximum values chosen for each factor. The factors are scaled so that the low level is assigned to a value of -1 and the high level is assigned to a value of +1. Factors are usually denoted by uppercase letters (interactions of factors are called words because they are denoted by the uppercase letters of the combined factors), lowercase letters are used for the high level of the factor, and the letter is omitted for the lower level. A complete trial requires $2x2\ldots x2=2^k$ observations, thus this type of design is called a 2^k design. Since only two levels are used for each factor, the response is assumed to be approximately linear over the chosen range of the factor levels. The statistical model for the general 2^k design includes $C_{k,1}$ combinations of main effects, $C_{k,2}$ combinations of two-factor interactions, $C_{k,3}$ combinations of three-factor interactions, $C_{k,4}$ combinations of four-factor interactions, and so on up to $C_{k,k}$ combinations of *k*-factor interactions [Montgomery-13].

For even a small number of factors, the total number of runs in a trial of a 2^k design is large. Sometimes the number of replicates that the experimenter is able to do is restricted due to limited resources, or because the experiment can only use simulation data. Because of this, occasionally only a single replicate of the design can be run. A risk when dealing with an unreplicated factorial experiment is that the model may be fitted to noise. This can be mitigated by increasing the distance between the low (-) and high (+) levels of the factors. Another problem with only one replicate, is that there is no internal estimate of statistical error [Montgomery-13].

Li, Sudarsanam, and Frey studied in [Li-06], a set of 46 published experiments from a variety of fields that included 113 response variables in all. They used a General Linear Model to estimate factor effects, all the experiments were full two-level factorials with between three and seven factors. They studied the effect sparsity in the 113 responses. In the study they found that more than a third of all main effects were classified as active (having an important influence on the response). Only about 7.4% of all two-factor interactions were active, and the percentage drops

as the number of factors in the interactions rise, thus providing evidence for the validity of the use of the effect sparsity principle in unreplicated designs. Effect sparsity is the observation that most systems are dominated by some of the main effects and low-order interactions [Li-06].

Using the effect sparsity principle it can be assumed that certain high-order interactions are negligible, and their mean squares can be combined to estimate the error. However, real high-order interactions can occasionally occur. When analyzing unreplicated designs, examining a normal probability plot of the estimate of the effects is recommended by Cuthbert Daniel [Daniel-59].

Daniel's method requires the experimenter to make a judgment about what is an outlier and what is not [Daniel-59]. To remove this element of subjectivity, Lenth proposes an objective method for deciding which effects are active in the analysis of unreplicated experiments [Lenth-89]. Lenth's method consists in estimating a standard-error-like quantity, called the pseudo standard error, or PSE, defined in (1-1). To find the critical value (the cutoff value) for statistically significant effects, the PSE is multiplied by a critical t-value with degrees of freedom equal to the total number of effects divided by 3, as in (1-2). The factor effects can then be plotted in a normal plot with a reference line having a slope equal to the PSE. The effects that are negligible are normally distributed, with mean zero and variance σ^2 and will tend to fall along the PSE line, whereas significant effects will have nonzero means and will not lie along the line [Lenth-89].

$$PSE = 1.5 \cdot median_{\{|c_i|<2.5s_0\}} |c_i| \tag{1-1}$$

$$critical\_value = PSE \cdot t_{0.05,df} \tag{1-2}$$

where

$$df = total\_effects/3 \tag{1-3}$$

$$S_0 = 1.5 \cdot median\ |c_i| \tag{1-4}$$

$$c_i = estimated\quad effects$$

When 3- and higher-factor interactions are considered negligible (making use of the effect sparsity principle), frequently half or more runs in a trial do not give useful information regarding the important effects of the factors and their interactions, and therefore are waste. In these cases, a fractional factorial design is used, where, as the name implies, only a fraction of the full factorial design is used. When all possible combinations of factors and levels are not evaluated in the experiment, certain factor and interaction effects will be confounded (or aliased) together, meaning the estimate of an effect includes the influence of one or more other effects and cannot be attributed

TABLE III
TYPES OF RESOLUTION FOR FRACTIONAL DESIGNS [Kuehl-01]

Type	Explanation
Resolution III	These are designs in which no main effects are aliased with any other main effect, but main effects are aliased with two-factor interactions, and two-factor interactions may be aliased with each other.
Resolution IV	These are designs in which no main effect is aliased with any other main effect or with any two-factor interactions, but two-factor interactions are aliased with each other.
Resolution V	These are designs in which no main effect or two-factor interaction is aliased with any other main effect or two-factor interaction, but two-factor interactions are aliased with three-factor interactions.

unambiguously to a single factor or interactions [Mason-03]. The experiment design chosen should allow a clear evaluation of main effects and interaction effects thought to be strong (especially 2-factor interactions since these are not usually considered negligible) [Box-05].

A fractional factorial design containing 2^{k-p} runs is called a $(1/2)^p$ fraction of the 2^k design, and requires p independent generators. A generator is a relationship between factors in a fractional factorial experiment that determines how the fraction of runs is selected from the full factorial design. The defining relation of a design is made of all the design generators, and is used to calculate the alias structure that describes the confounding in the fractional factorial design [Support.minitab-15]. A reasonable criterion is to select the generators such that the resulting 2^{k-p} design has the highest possible resolution. A design is of resolution R if no p-factor effect is aliased with another effect containing less than $R - p$ factors. In general, the resolution of a two-level fractional factorial design is equal to the number of letters (factors) in the shortest word in the defining relation [Montgomery-13]. TABLE III lists the most common types of resolutions available.

1.3. Design of Experiments for the Selected Topology

The time that takes the signal to go through all the components starting from the master all the way to the slave, is called flight time, and is a function of the propagation delay of the components as in (1-5) (see Fig. 1-2) [Balasubramaniam-01]. The flight time for the system studied here is a function of the propagation delay of the series resistors, and the propagation delay and length of the transmission lines. This last delay is a function of the characteristic impedance of the transmission lines per unit length.

$$t_{fllight} = t_{pd\_L1} \cdot length\_of\_L1 + t_{pd\_resistor} + t_{pd\_L2} \cdot length\_of\_L2 \quad (1\text{-}5)$$

The uncontrollable design factors in TABLE II affect the propagation delay of the different components, and thus have an effect on the overall flight time of the system. In this work, a screening experiment is performed in order to identify those uncontrollable factors that have the most influence on the flight time of the system. The transmission line lengths are considered fixed for the purpose of the screening experiment, at 2.5 in for L1, and 3.5 in for L2.

Based on the factors in TABLE II, if a full 2^5 factorial design were chosen for this screening experiment, 32 runs of the experiment would be needed. As explained above, this means 16 out of the total 32 runs ($C_{5,3}$ three-factor interactions, $C_{5,4}$ four-factor interactions, and one 5-factor interaction) are waste if the effect sparsity principle is used. For this reason a 2^{5-1} fractional factorial design is chosen for the experiment, since it is a Resolution V design. For this 2^{5-1} design the generator chosen is $E = ABCD$ (the other option for the generator in a 2^{5-1} design is $E = -ABCD$).

For this work, factor and interaction effects are calculated with JMP® Pro 9.0.3 statistical software[1]. As explained before, the factors are denoted by uppercase letters, lowercase letters are used for the high level of the factor and the letter is omitted for the lower level. When all the factors are at the lower level, the symbol (1) is used. It is often convenient to write down the treatment combinations (combination of the levels of the factors) in standard order or Yate's order, starting with (1), then putting one letter at a time followed by all combinations with letters that have been previously added [Dodge-08]. This translates into writing in the *k*-th column of the design, 2^{k-1} minus signs followed by 2^{k-1} plus signs [NIST/SEMATECH-15].

The design for this experiment is constructed by writing down the design for a full 2^{5-1} factorial in Yate's order. The generator chosen for the design is then solved for the missing column

[1] JMP®, Version Pro 9.0.3, 2011, SAS Institute Inc., Cary, NC.

of the design (corresponding to the E factor). TABLE IV shows the design generated in JMP® for

TABLE IV
DESIGN TABLE FOR SCREENING EXPERIMENT

Run	Pattern		A (slave_ corner)	B (resistor value)	C (Zo board TLs)	D (master_ corner)	E=ABCD (Zo PKG TLs)
1	(1)	−−−− +	-1	-1	-1	-1	1
2	a	+−−−−	1	-1	-1	-1	-1
3	b	−+−− −	-1	1	-1	-1	-1
4	ab	++−− +	1	1	-1	-1	1
5	c	−−+− −	-1	-1	1	-1	-1
6	ac	+−+− +	1	-1	1	-1	1
7	bc	−++− +	-1	1	1	-1	1
8	abc	+++− −	1	1	1	-1	-1
9	d	−−−+ −	-1	-1	-1	1	-1
10	ad	+−−+ +	1	-1	-1	1	1
11	bd	−+−+ +	-1	1	-1	1	1
12	abd	++−+ −	1	1	-1	1	-1
13	cd	−−++ +	-1	-1	1	1	1
14	acd	+−++ −	1	-1	1	1	-1
15	bcd	−+++ −	-1	1	1	1	-1
16	abcd	++++ +	1	1	1	1	1

the 2^{5-1} screening design.

1.4. Flight Time Measurement

To measure flight time, intuitively a probe would be set at the driver's output and another at the receiver's input, and the flight time would be the difference in time between these two points. However, there are reflections that bounce back to the driver, resulting in a degraded signal at the driver's output. If the flight time were measured from this point, it would be an incorrect measurement. Flight time in simulation is more accurately defined as "the amount of time that elapses between the point where the signal on an output buffer driving a reference load crosses the threshold voltage and the time where the signal crosses the threshold voltage at the receiver in the system" [Hall-00]. This means, a simulation reference load is required to measure the flight time

correctly. Fig. 1-4 a) shows the placement of probes on the topology for the simulation and the waveform of the signal at each probe. Fig. 1-4 b) shows the difference between the waveform at the driver's output, and the waveform at the reference load.

The receiver buffers in a digital system are designed to distinguish between a high and a low logic state at a threshold voltage. However, due to process variations and system noise, the threshold voltage may change. This variation produces a threshold region that typically extends 100 to 200 mV above and below the threshold voltage. The upper and lower limits of the threshold region are referred to as *VIH* and *VIL*, respectively. To ensure the integrity of the data being transmitted, the system must be able to deliver high logic states that remain above *VIH*, and low logic states that remain below *VIL* [Hall-00].

The flight time should be evaluated at *VIL*, $V_{threshold}$, and *VIH* according to Fig. 1-5 and (1-6), where only the worst case (largest value) of the three measurements is used. When using the flight times in time-margin equations, the worst case flight time should be inserted. However in practice, for simplicity flight time is measured only at one threshold, usually at $V_{threshold}$ or at *VIH*, depending on the behavior of the signal. For the system analyzed in this work, the flight time is measured at $V_{threshold}$, since measuring at *VIH* is very pessimistic, and can limit unrealistically the solution space of the system.

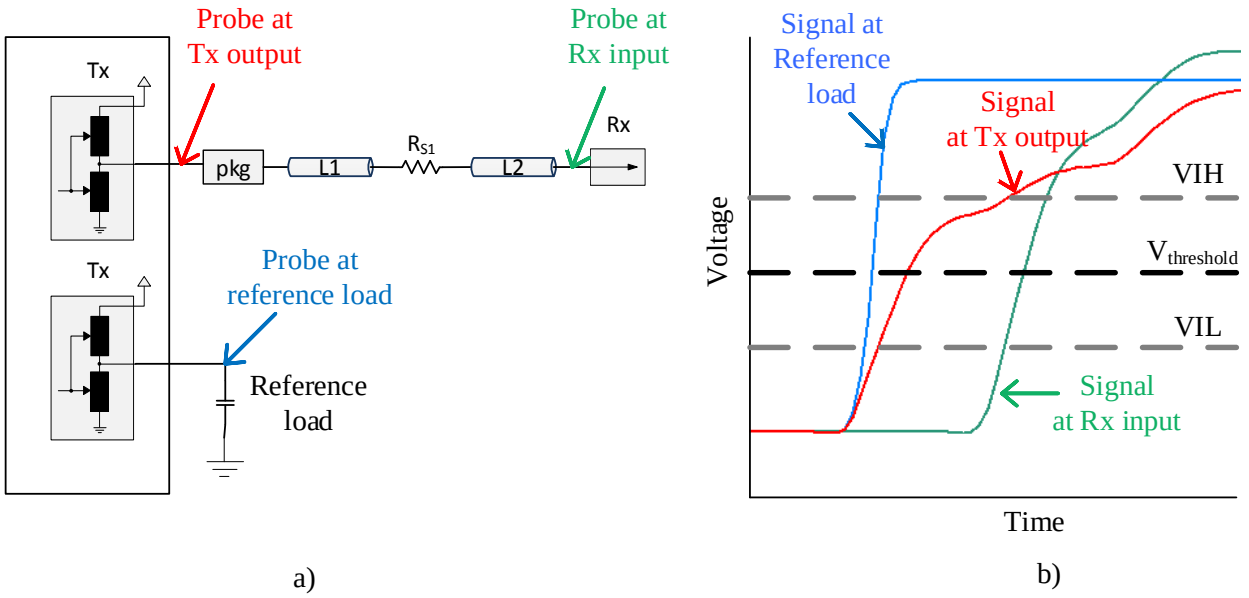

Fig. 1-4 Flight time measurement. a) Placement of probes for simulation b) waveforms of the signal at probes.

1. SCREENING EXPERIMENT

After the 16 runs from TABLE IV are simulated, the flight times are measured from the simulation results, and are introduced into JMP® as the response of the system, in order to calculate the estimated factor effects. TABLE V shows the calculated effect estimates from JMP®

$$t_{fllight} = Worst\ case \begin{cases} T_{h\_rx} - T_{h\_ref} \\ T_{m\_rx} - T_{m\_ref} \\ T_{l\_rx} - T_{l\_ref} \end{cases} \tag{1-6}$$

The data for this experiment comes from simulation. As previously explained, this means that only one replicate of the design can be obtained since further replicates will result in the exact same data. Therefore high-order interactions are considered negligible and used to calculate the statistical error. To verify that those high-order interactions can indeed be considered negligible, Lenth's method is followed to construct a normal probability plot of the estimated effects.

First, the estimated effects in TABLE V are sorted into increasing order of the absolute values excluding the intercept effect. The median of the new list in TABLE VI is then multiplied by 1.5 according to (1-4).

$$s_0 = 1.5 \cdot median|c_i| = 1.5 \cdot 0.004922 = 0.007383$$

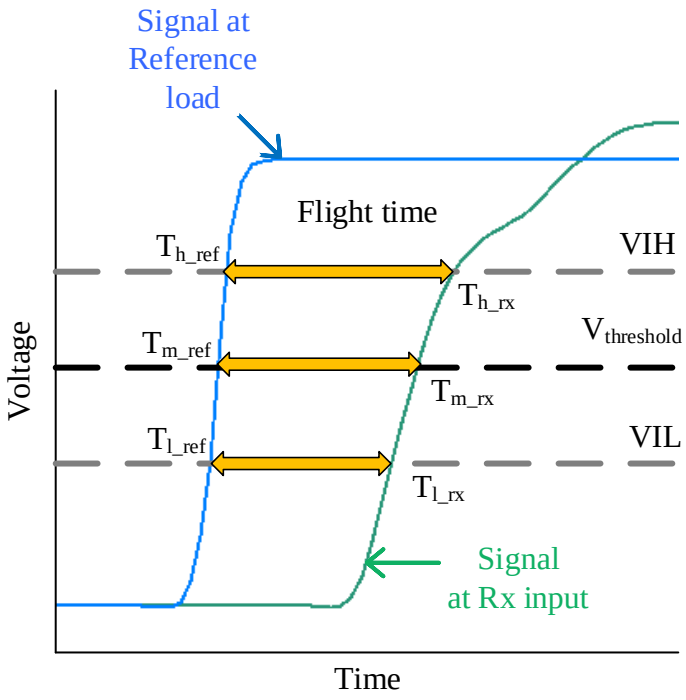

Fig. 1-5 Flight time measurement in waveforms.

TABLE V
FACTOR EFFECTS CALCULATED WITH JMP®

Term	Estimate
Intercept	1.649283
A	0.032367
B	0.009993
C	-0.05322
D	-0.17275
E	-0.00401
A*B	0.001479
A*C	-0.00526
A*D	-0.01649
A*E	0.001162
B*C	-0.00191
B*D	-0.00492
B*E	0.003663
C*D	0.028695
C*E	-0.00142
D*E	0.000755

Lenth takes this value as a preliminary estimate and refines the effects lists by excluding all effects exceeding 2.5 times this estimate.

$$2.5 \cdot s_0 = 0.018458$$

Excluding factors with estimated effect larger than 0.018458 gives TABLE VII. The median of the remaining effects is multiplied by 1.5 to obtain the PSE value. The PSE is multiplied by a critical t-value ($t_{0.05,df}$) with degrees of freedom equal to the total number of effects divided by 3, according to (1-2) and (1-3).

1. SCREENING EXPERIMENT

$$PSE = 1.5 \cdot median_{\{|c_i| \langle 2.5 s_0 \}} |c_i| = 1.5 \cdot 0.003663 \quad = 0.00549$$

$$\deg rees\_ freedom = df = 15/3 = 5$$

$$t_{0.05,5} = 2.015$$

$$critical\_value = PSE \cdot t_{0.05,5} = 0.011072$$

All factors and interactions with effects smaller than the critical value of 0.011072 are negligible in the design; factors A, C, D, and the interactions AD and CD have significant effects, and the rest of the factors and interactions can be considered negligible as they fall along the reference line having a slope equal to the PSE. Therefore, slave_corner, Zo of the board transmission lines, and master_corner are the active factors in this design.

For the digital signal coming from the slave buffer, a screening experiment was performed similar to the one previously explained for the master signal to see which of the uncontrollabe factors in TABLE II are negligible for the design. The design table for this experiment is the same as TABLE IV. TABLE IX shows the estimated screening factor effects calculated for the signal coming from the slave buffer. As previously explained, Lenth's method is followed to decide which parameters can be considered negligible for further experiments. The critical value from Lenth's method is 0.010068, meaning only the factors A, C, D, E, and interactions AD, CD, have significant effects, while the rest of the factors and interactions can be considered negligible. Therefore, master_corner, Zo of the board transmission lines, slave_corner, and Zo of the package transmission lines are the active factors in this design. For further experiments, six factors in total will be used for the slave signal model, the four active factors plus the lengths L1 and L2.

TABLE VI
FACTOR EFFECTS SORTED INCREASINGLY

Term	Absolute value of estimate
D*E	0.000755
A*E	0.001162
C*E	0.001417
A*B	0.001479
B*C	0.001913
B*E	0.003663
E	0.004011
B*D	0.004922
A*C	0.005263
B	0.009993
A*D	0.016494
C*D	0.028695
A	0.032367
C	0.05322
D	0.172745
median	0.004922

TABLE VII
EFFECTS SMALLER THAN $2.5 \cdot s_0$

Term	Absolute value of estimate
D*E	0.000755
A*E	0.001162
C*E	0.001417
A*B	0.001479
B*C	0.001913
B*E	0.003663
E	0.004011
B*D	0.004922
A*C	0.005263
B	0.009993
A*D	0.016494
median	0.003663

TABLE VIII
SCREENING FACTOR EFFECTS FOR THE MISO DATA LINE
CALCULATED WITH JMP®

Term	Estimate
Intercept	1.6619301
A	0.0292255
B	0.0099757
C	-0.049679
D	-0.167983
E	-0.013259
A*B	0.0008955
A*C	-0.004626
A*D	-0.015952
A*E	0.000396
B*C	-0.001715
B*D	-0.004401
B*E	0.003331
C*D	0.0271223
C*E	-0.000433
D*E	0.0026336

1.5. Conclusions

In this chapter, the uncontrollable and controllable factors were chosen for the system being studied. From the uncontrollable factors of the system, the ones with significant main effects on the flight times of the signal coming from the buffers were identified using screening experiments. These experiments provided information only on the direct additive effects and pairwise interactions effects of the factors. No replication was used in the experiments, as the data used came from SPICE simulations. For this reason, Lenth's method for unreplicated experiments was followed to decide which factors could be considered to have a negligible effect on the response of the system.

From the five uncontrollable factors chosen to be investigated, three were concluded to have active effects on the flight time of the master, i.e., the operating conditions of both buffers and the characteristic impedance of the PCB transmission lines. These three factors were also determined to have active effects on the flight time of the slave signal, along with the characteristic impedance of the package transmission lines.

2. The Surrogate Model

The screening experiments done so far consist of trial runs at the lower-bound and upper-bound level setting combinations of the ranges of the factors, providing information on the direct additive effects of the variables and pairwise interactions effects [Verseput-00]. Once the main design factors have been selected in the screening experiment, the next step is to fit a mathematical model to the data that represents the system.

2.1. Constructing the Model

It is a good idea that the design selected provide curvilinear factor effects in addition to the direct additive and interaction effects, in case the system does not present a linear behavior. This cannot be done with a linear design, and thus a second-order model in the form of (2-1) is needed [Myers-02].

$$y = \beta_0 + \sum_{i=1}^{k} \beta_i x_i + \sum_{i=1}^{k} \beta_{ii} x_i^2 + \sum_{i<j}^{k-1} \sum_{j=2}^{k} \beta_{ij} x_i x_j + \varepsilon \tag{2-1}$$

where x are the design variables, k is the number of design variables, y is the predictor that involves the design variables, ε represents the error in the system, and β the regression coefficients.

To determine the parameters of the quadratic regression in (2-1) a design needs to have at least three levels for each factor and $1+2k+k(k-1)/2$ runs [Myers-02]. 3^k factorial designs can be used to estimate quadratic regression models, however the number of runs required in this type of designs can be huge, making the design ultimately impractical. A popular type of second-order design is the Central Composite Design (CCD). This experimental scheme uses a 2^k complete or resolution V fractional factorial, combined with n_c center points, plus $2k$ axial points where the parameters are given in terms of a distance from the central point called the axial distance α; TABLE IX lists the axial points. The center runs provide information about the curvature of the system and can be used for an internal estimate of statistical error. If curvature is found in the system, the axial points allow an efficient estimation of the quadratic terms [Myers-02].

TABLE IX
AXIAL POINTS FOR CCD [Myers-02]

x_1	x_2	⋯	x_k
$-\alpha$	0	…	0
α	0	…	0
0	$-\alpha$	…	0
0	α	…	0
⋮	⋮		⋮
0	0	…	$-\alpha$
0	0	…	α

It is important for the second order model to provide good predictions throughout the region of interest. One way to ensure this is to require that the model have a consistent and stable variance of the predicted response throughout the region of interest, in other words, that the design be rotatable. A CCD can be made rotatable by choosing α as (2-2).

$$\alpha = (n_f)^{1/4} \tag{2-2}$$

where n_f is the number of points used in the factorial portion of the design [Montgomery-13].

In a rotatable CCD, all points at the same distance from the center point have the same prediction error; factorial and axial points fall on different concentric spheres and in consequence have different prediction error.

It is not important to have exact rotatability in a design. If the region of interest is found to be spherical, a good choice of α is to set it at

$$\alpha = \sqrt{k} \tag{2-3}$$

where *k* is the number of factors. This value of α puts all the factorial and axial points on the surface of a sphere of radius $\sqrt{k}$ [Montgomery-13].

Another choice of the axial distance is α=1. This is used when the region of interest and the region of operability are the same, so the axial points occur at the center of the faces rather than outside as it happens in a spherical region, resulting in a face-centered cube design [Kuehl-01].

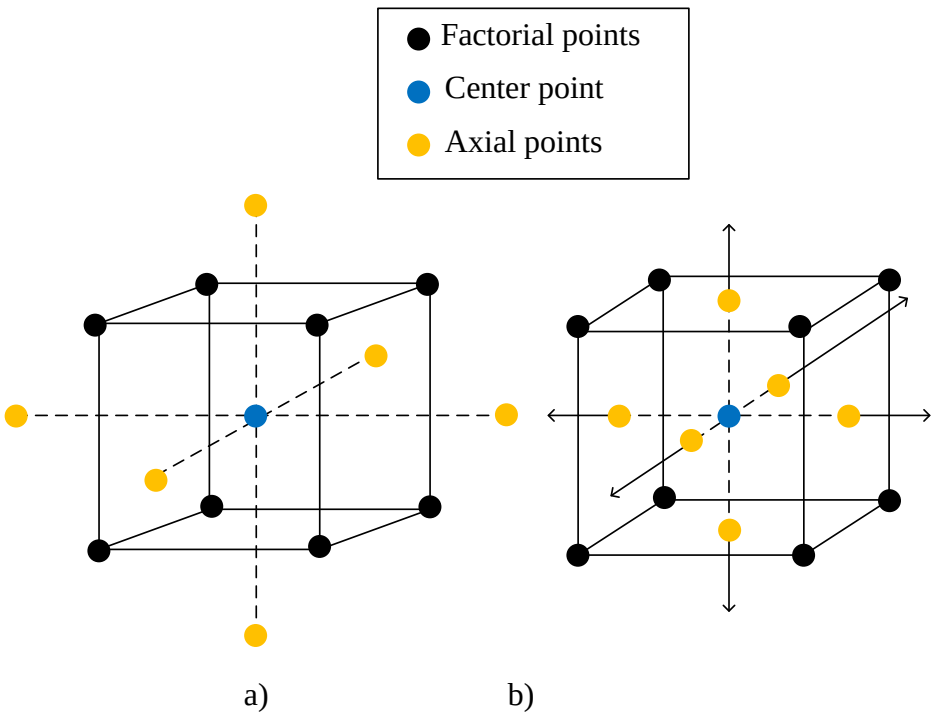

Fig. 2-1 Types of central composite designs. a) Rotatable CCD if $\alpha = (n_f)^{1/4}$ Spherical CCD if $\alpha = \sqrt{k}$ b) Face-centered CCD

Rotatable and spherical designs allow uniform prediction error and extension of the design region, but require 5 levels for each factor. Face-centered designs are less complex, they require only 3 levels of each factor, but are not as powerful at extrapolating predictions. Fig. 2-1 shows the geometry of rotatable, spherical, and face-centered designs.

In a central composite design, each factor has the high level (+1) and low level (-1) from the factorial design. In addition to these levels, each factor has an intermediate level (0) that corresponds to the nominal value of the factor, and two new levels are added that correspond to the axial distances -α and +α.

A second-order regression model is fitted to the system to represent the flight time of the digital signal coming from the master buffer of Fig. 1-2 using a CCD. From the screening experiment performed using the point-to-point topology, slave_corner, Zo of the board transmission lines, and master_corner were determined to be the active factors in the design, and the lengths of the PCB transmission lines, the values for L1 and L2 were fixed. The distance between master and slave is the largest factor in the flight time, and is dependent on the length of the transmission lines of the interconnection, L1 and L2. Thus, the regression model in this work

2. THE SURROGATE MODEL

TABLE X
DESIGN FACTORS FOR CCD

Factor
master_corner
slave_corner
Zo of board routing
Length of L1
Length of L2

is required to consider the lengths L1 and L2 as design variables in addition to the design factors chosen from the screening experiment. TABLE X shows the variables used in the CCD experiment for the master signal.

For the CCD experiment a Resolution V design is chosen as it requires fewer runs than the complete design and will still result in an adequate regression model. One center point is used for the experiment as the data for the experiment comes from simulation only. The design for this experiment is constructed by writing down the design for a 2^{5-1} factorial, the 10 axial points, and the central point. For easiness in the analysis, when dealing with master_corner and slave_corner factors, the voltage value of the corresponding operating conditions will be used.

For a 2^{5-1} CCD it doesn't matter if the design is completely rotatable or assumed to be spherical, because using (2-2) and (2-3), the value of α is the same in both assumptions. For a rotatable design: $\alpha=(2^{5-1})^{1/4}=2$, and for a spherical design: $\alpha = \sqrt{4} = 2$.

A quadratic regression model will be fitted to the system in Fig. 1-2 using α=2 and then using α=1 to see what kind of design better fits the system.

TABLE XI
DESIGN FACTORS AND LEVELS FOR THE CENTRAL COMPOSITE DESIGN FOR THE TX SIGNAL

Factor	Symbol	Value at $-\alpha$ = -2	Value at -1	Value at 0	Value at +1	Value at $+\alpha$ = 2
slave_corner	A	2.97V	3.13V	3.3V	3.465V	3.63V
master_corner	B	2.97V	3.13V	3.3V	3.465V	3.63V
Zo of board routing	C	42ohm	46ohm	50ohm	54ohm	58ohm
Length of L1	D	0.01in	2.005in	4in	5.995in	7.99in
Length of L2	E	0.01in	3.505in	7in	10.495in	13.99in

TABLE XII
DESIGN TABLE FOR THE ROTATABLEL CCD EXPERIMENT FOR THE TX SIGNAL

Run	Pattern	A (slave_ corner)	B (master_ corner)	C (Zo of board routing)	D (Length of L1)	E (Length of L2)
1	−−−− −	-1	-1	-1	-1	-1
2	+−−− +	1	-1	-1	-1	1
3	−+−− +	-1	1	-1	-1	1
4	++−− −	1	1	-1	-1	-1
5	−−+− +	-1	-1	1	-1	1
6	+−+− −	1	-1	1	-1	-1
7	−++− −	-1	1	1	-1	-1
8	+++− +	1	1	1	-1	1
9	−−−+ +	-1	-1	-1	1	1
10	+−−+ −	1	-1	-1	1	-1
11	−+−+ −	-1	1	-1	1	-1
12	++−+ +	1	1	-1	1	1
13	−−++ −	-1	-1	1	1	-1
14	+−++ +	1	-1	1	1	1
15	−+++ +	-1	1	1	1	1
16	++++ −	1	1	1	1	-1
17	a0000	-2	0	0	0	0
18	A0000	2	0	0	0	0
19	0a000	0	-2	0	0	0
20	0A000	0	2	0	0	0
21	00a00	0	0	-2	0	0
22	00A00	0	0	2	0	0
23	000a0	0	0	0	-2	0
24	000A0	0	0	0	2	0
25	0000a	0	0	0	0	-2
26	0000A	0	0	0	0	2
27	0	0	0	0	0	0

Starting with the design where α=2, TABLE XI shows the design levels for each of the factors, and TABLE XII shows the experiment design generated in JMP®. When the 27 simulation

runs from TABLE XII are completed, the flight times are measured from the simulation results and are introduced into JMP® as the response of the system. In a central composite design, the estimates calculated with JMP® are considered the regression model coefficients, instead of the effect estimates as in a screening experiment. TABLE XIII shows the calculated estimated regression coefficients.

From (2-1) and the coefficients in TABLE XIII , the quadratic regression model for the design with $\alpha=2$ of the system in Fig. 1-2 is shown in (2-4).

TABLE XIII
REGRESSION ESTIMATED COEFFICIENTS FOR THE ROTATABLE CCD EXPERIMENT FOR THE TX SIGNAL

Term	Estimate
Intercept	2.444906
A	0.029035
B	-0.12862
C	-0.05867
D	0.362372
E	0.632873
A*B	-0.01763
A*C	-0.00512
B*C	0.030336
A*D	0.000382
B*D	-0.00681
C*D	-0.00577
A*E	-0.00031
B*E	-0.00897
C*E	-0.00781
D*E	-0.00326
A*A	0.017206
B*B	0.0214
C*C	0.020996
D*D	0.017288
E*E	0.01124

$$\begin{aligned} FlightTime_{Tx\_rotatable} = {} & 2.444 + 0.029\ A - 0.128\ B - 0.059\ C + 0.362\ D + 0.632\ E - \\ & 0.0176\ AB - 0.00512\ AC + 0.0303\ BC + 0.000382\ AD - \\ & 0.00681\ BD - 0.00577\ CD - 0.00031\ AE - 0.00897\ BE - \\ & 0.00781\ CE - 0.00326\ DE + 0.0172\ AA + 0.0214\ BB + \\ & 0.02099\ CC + 0.01728\ DD + 0.01124\ EE \end{aligned} \tag{2-4}$$

Before accepting the regression model in (2-4) as an adequate model for the system being studied, the model fit must be evaluated. "A well-fitted regression model will result in predicted values close to the observed data values" [Grace-Martin-15]. JMP® provides an Actual by Predicted plot that shows how well the model fits the data. This type of plot shows the actual response values versus the response values predicted by the models. JMP® also provides the value for the main statistics to evaluate model fit: P-value, R-squared (*RSq*), and RMSE. All three are based on the total sum of squares (SST) that measures how far the observed data is from the mean, and the sum of squares error (SSE) that measures how far the observed data is from the predicted values. If there are *a* levels for each factor, and *n* observations under the *i*-th treatment, SSE and SST are calculated according to (2-5) and (2-6) [Montgomery-13]

$$SSE = \sum_{i=1}^{a}\sum_{j=1}^{n}\left(y_{ij} - \bar{y}_{i.}\right)^2 \tag{2-5}$$

$$SST = \sum_{i=1}^{a}\sum_{j=1}^{n}\left(y_{ij} - \bar{y}_{..}\right)^2 \tag{2-6}$$

where y_{ij} is the *j*-th observation taken under the factor level *i*, $\bar{y}_{i.}$ represents the average of the observations under the *i*-th treatment, and $\bar{y}_{..}$ represents the grand average of all observations. Note that the "dot" subscript implies summation over the subscript that it replaces [Montgomery-13].

R-squared (*RSq*) is the percentage of variance in the response accounted for by the model. It ranges from zero to one, with zero indicating that the model does not predict well, and 1 indicating perfect prediction. R-squared is calculated according to (2-7) [Montgomery-13].

$$RSq = 1 - \frac{SSE}{SST} \tag{2-7}$$

A disadvantage with the *RSq* is that every time a predictor is added to the model, the *RSq* value will always increase, and the model may appear to have a better fit. As more predictors are

added to the model looking for a better *RSq*, it begins to model random noise in the data, producing a high *RSq* with bad predictability. This is where the adjusted R-squared comes in. It is a modified version of *RSq* that has been adjusted for the number of predictors in the model. It will increase only if the term added improves the model, and will actually decrease if the model is not improved by the new term. The adjusted R-squared ($RSq_{(adj)}$) will always be smaller than the R-squared and is calculated according to (2.8) [Allen-10]

$$RSq_{(adj)} = 1 - \left(\frac{n-1}{n-k}\right)\left(\frac{SSE}{SST}\right) \tag{2-8}$$

The P-value is related to the F-test, which evaluates the null hypothesis that all regression coefficients are equal to zero, meaning it is an intercept-only model, as opposed to the alternative that at least one coefficient is not. It indicates if the *RSq* value is reliable. A low P-value indicates the null hypothesis can be rejected, meaning the model does provide a better fit than an intercept-only model would [Grace-Martin-15].

The RMSE is the square root of the mean square error. It is a measure of the stochastic component or error, and estimates the concentration of the observed data around the fitted equation. A large value of RMSE implies that a large amount of variance in the dependent variable is not explained by the model, therefore lower values indicate a better fit [Grace-Martin-15].

Fig. 2-2 shows the Actual by Predicted plot generated in JMP® for the rotatable CCD experiment using α=2. This plot shows the actual flight time values measured from SPICE simulations, and the flight time values predicted by the rotatable model. The red diagonal line is the line of fit; it shows where the simulated flight times are identical to the predicted ones. The dashed horizontal blue line is set at the mean of the simulated flight times. The dashed red curves are the confidence bands for the mean [Jmp-16]. JMP® also provides a summary of fit, where *RSq* is 0.987, $RSq_{(adj)}$ is 0.942, and the RMSE is 0.173. From these values, it can be accepted that the model has an acceptable fit.

TABLE XIV
DESIGN FACTORS AND LEVELS FOR CCD WITH $\alpha = 1$

Factor	Symbol	Value at $-\alpha$ = -1	Value at 0	Value at $-\alpha$ =+1
master_corner	A	3.135V	3.3V	3.465V
slave_corner	B	3.135V	3.3V	3.465V
Zo of board routing	C	46ohm	50ohm	54ohm
Length of L1	D	0.01in	4in	7.99in
Length of L2	E	0.01in	7in	13.99in

TABLE XIV shows the design levels for each of the factors for the face-centered design where α=1, and TABLE XV shows the experiment design generated in JMP®. As before, when the 27 simulation runs from TABLE XV are completed, the flight times are measured from the simulation results and are introduced into JMP® as the response of the system. TABLE XVI shows the calculated estimated regression coefficients

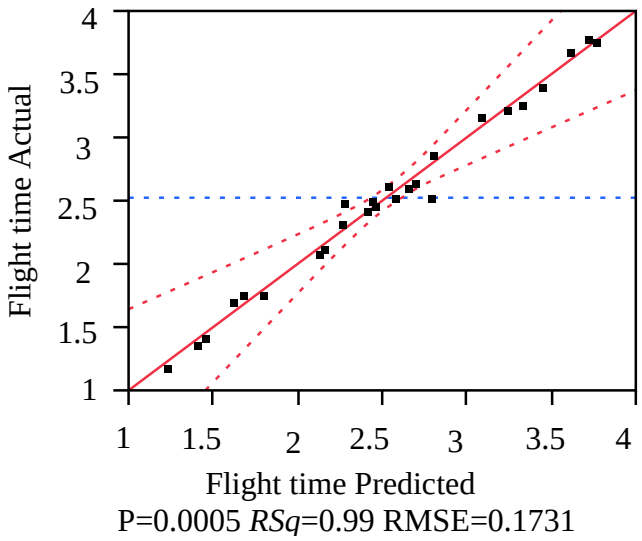

Fig. 2-2 Actual by Predicted plot generated in JMP® for the signal coming from the master buffer for the rotatable CCD. The red diagonal line is the line of fit, the dashed horizontal blue line is set at the mean of the simulated flight times, and the dashed red curves are the confidence bands for the mean [Jmp-16].

TABLE XV
DESIGN TABLE FOR THE CCD EXPERIMENT WITH $\alpha = 1$

Run	Pattern	A (slave_ corner)	B (master_ corner)	C (Zo of board routing)	D (Length of L1)	E (Length of L2)
1	−−−− −	-1	-1	-1	-1	-1
2	+−−− +	1	-1	-1	-1	1
3	−+−− +	-1	1	-1	-1	1
4	++−− −	1	1	-1	-1	-1
5	−−+− +	-1	-1	1	-1	1
6	+−+− −	1	-1	1	-1	-1
7	−++− −	-1	1	1	-1	-1
8	+++− +	1	1	1	-1	1
9	−−−+ +	-1	-1	-1	1	1
10	+−−+ −	1	-1	-1	1	-1
11	−+−+ −	-1	1	-1	1	-1
12	++−+ +	1	1	-1	1	1
13	−−++ −	-1	-1	1	1	-1
14	+−++ +	1	-1	1	1	1
15	−+++ +	-1	1	1	1	1
16	++++ −	1	1	1	1	-1
17	a0000	-1	0	0	0	0
18	A0000	1	0	0	0	0
19	0a000	0	-1	0	0	0
20	0A000	0	1	0	0	0
21	00a00	0	0	-1	0	0
22	00A00	0	0	1	0	0
23	000a0	0	0	0	-1	0
24	000A0	0	0	0	1	0
25	0000a	0	0	0	0	-1
26	0000A	0	0	0	0	1
27	0	0	0	0	0	0

TABLE XVI
REGRESSION ESTIMATED COEFFICIENTS FOR CCD WITH $\alpha = 1$

Term	Estimate
Intercept	3.6429211
A	0.0319181
B	-0.134997
C	-0.047024
D	1.5370699
E	1.5214034
A*B	-0.015726
A*C	-0.020587
B*C	0.0067479
A*D	0.0027028
B*D	-0.023491
C*D	-0.01779
A*E	0.0066554
B*E	-0.01104
C*E	-0.014589
D*E	-0.022106
A*A	0.0005425
B*B	0.0626414
C*C	-0.029485
D*D	-0.040775
E*E	-0.10486

From (2-1) and the coefficients in TABLE XVI, the quadratic regression model with α=1 of the system in Fig. 1-2 is shown in equation (2-9).

$$\begin{aligned} FlightTime_{Tx\_face-centered} = {} & 3.643 + 0.032\ A - 0.1349\ B - 0.047\ C + 1.537\ D + \\ & 1.521\ E - 0.0157\ AB - 0.02059\ AC + 0.00675\ BC + \\ & 0.0027\ AD - 0.0235\ BD - 0.0178\ CD + 0.00665\ AE - \\ & 0.01104\ BE - 0.0146\ CE - 0.02211\ DE + 0.000542\ AA + \\ & 0.06264\ BB - 0.02949\ CC - 0.040775\ DD - 0.10486\ EE \end{aligned} \tag{2-9}$$

Fig. 2-3 shows the Actual by Predicted plot generated in JMP® for the CCD experiment. From the values that JMP® gives for model fit – *RSq* of 0.9999, *RSq*(*adj*) of 0.9996, RMSE of 0.0227 – the model fit can be assumed adequate, and better than the model with α=2.

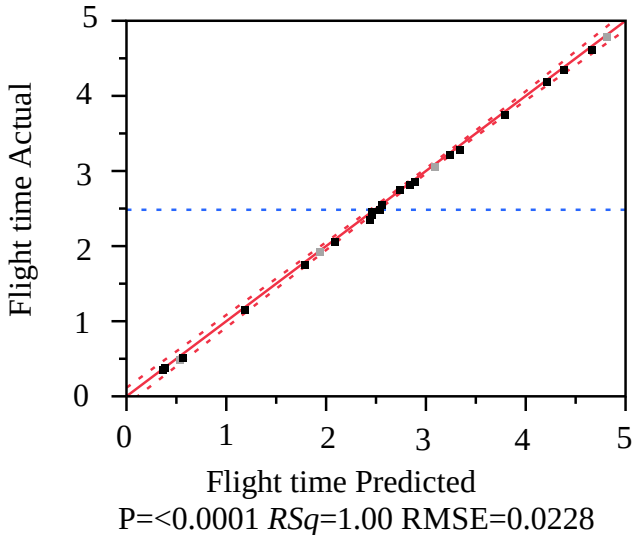

Fig. 2-3 Actual by Predicted plot generated in JMP® for the signal coming from the master buffer for the face-centered CCD. The red diagonal line is the line of fit, the dashed horizontal blue line is set at the mean of the simulated flight times, and the dashed red curves are the confidence bands for the mean [Jmp-16].

A second-order regression model is also fitted to the slave signal, using both a rotatable and a face-centered central-composite designs. Using (2-2), for a rotatable design of six factors, an alpha of 2.378 will be used.

Fig. 2-4 shows the Actual by Predicted plot generated in JMP® for the rotatable design, with an *RSq* of 0.991527, an *RSq*(*adj*) of 0.9781, and an RMSE of 0.1376. The rotatable regression model for the slave signal is shown in (2-10).

$$\begin{aligned} FlightTime_{Rx\_rotatable} = {} & 3.5525 - 0.155\ A + 0.035\ B - 0.076\ C + 0.647\ D + \\ & 0.646\ E - 0.013\ F - 0.0208\ AB + 0.0347\ AC - \\ & 0.0071\ BC - 0.0156\ AD + 0.0031\ BD - 0.0114\ CD - \\ & 0.0130\ AE + 0.0028\ BE - 0.01097\ CE + 0.00556\ DE + \\ & 0.00312\ AF - 0.0012\ BF + 0.000227\ CF - 0.00108\ DF - \\ & 0.00127\ EF + 0.013584\ AA + 0.01229\ BB + 0.016717\ CC + \\ & 0.01326\ DD + 0.009988\ EE + 0.013548\ FF \end{aligned} \tag{2-10}$$

Fig. 2-5 shows the Actual by Predicted generated for the face-centered design, with an *RSq* of 0.99974, an $RSq_{(adj)}$ of 0.999327, and an RMSE of 0.0512. The face-centered regression model for the slave signal is shown in (2-11).

$$\begin{aligned} FlightTime_{Rx\_face-centered} = {} & 3.5802 - 0.162\ A + 0.033\ B - 0.059\ C + \\ & 1.582\ D + 1.579\ E - 0.0156\ F - 0.0170\ AB + \\ & 0.0183\ AC - 0.00586\ BC - 0.0633\ AD + \\ & 0.0147\ BD - 0.0359\ CD - 0.05293\ AE + \\ & 0.01054\ BE - 0.03233\ CE + 0.0475\ DE + \\ & 0.0055047\ AF - 0.003985\ BF + 0.00487\ CF - \\ & 0.00219\ DF - 0.004579\ EF + 0.04742\ AA + \\ & 5.57E-05\ BB - 0.023057\ CC + 0.008688\ DD - \\ & 0.00983\ EE - 0.000337\ FF \end{aligned} \tag{2-11}$$

Table TABLE XVII shows the estimated regression coefficients for the rotatable designs for the slave signal (using α=2), and the master signal (using α=2.378) lines. TABLE XVIII shows the estimated regression coefficients for the face-centered designs for the master and slave signals.

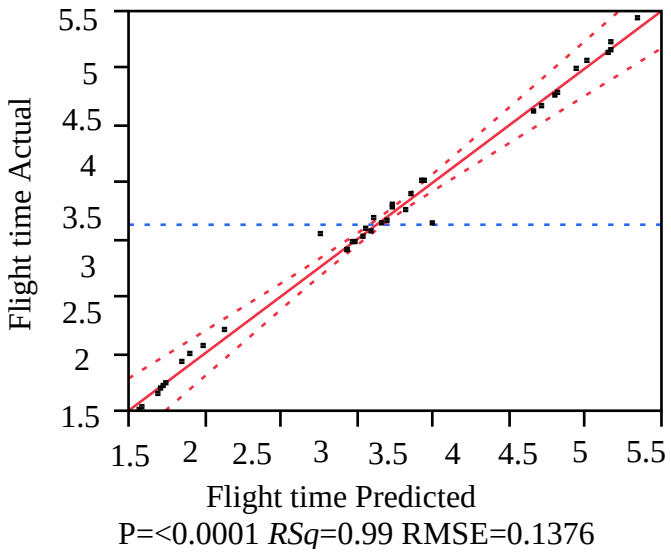

Fig. 2-4 Actual by Predicted plot generated in JMP® for the rotatable design for the slave signal. The red diagonal line is the line of fit, the dashed horizontal blue line is set at the mean of the simulated flight times, and the dashed red curves are the confidence bands for the mean [Jmp-16].

TABLE XVII
REGRESSION ESTIMATED COEFFICIENTS FOR THE ROTATABLE CCD EXPERIMENT FOR THE TX AND RX SIGNAL

$\alpha = 2$		$\alpha = 2.378$	
Clock/MOSI		MISO	
Term	Estimate	Term	Estimate
Intercept	2.444906	Intercept	3.552567
A	0.029035	A	-0.15534
B	-0.12862	B	0.034939
C	-0.05867	C	-0.07604
D	0.362372	D	0.647463
E	0.632873	E	0.645641
A*B	-0.01763	F	-0.01272
A*C	-0.00512	A*B	-0.02079
B*C	0.030336	A*C	0.034663
A*D	0.000382	B*C	-0.00711
B*D	-0.00681	A*D	-0.01559
C*D	-0.00577	B*D	0.003138
A*E	-0.00031	C*D	-0.01114
B*E	-0.00897	A*E	-0.01301
C*E	-0.00781	B*E	0.0028
D*E	-0.00326	C*E	-0.01097
A*A	0.017206	D*E	0.005557
B*B	0.0214	A*F	0.003123
C*C	0.020996	B*F	-0.0012
D*D	0.017288	C*F	0.000227
E*E	0.01124	D*F	-0.00108
		E*F	-0.00127
		A*A	0.013584
		B*B	0.012294
		C*C	0.016717
		D*D	0.01326
		E*E	0.009988
		F*F	0.013548

TABLE XVIII
REGRESSION ESTIMATED COEFFICIENTS FOR THE FACE-CENTERED CCD EXPERIMENT FOR THE TX AND RX SIGNAL

$\alpha = 1$			
Clock/MOSI		MISO	
Term	Estimate	Term	Estimate
Intercept	3.6429211	Intercept	3.5802104
A	0.0319181	A	-0.16224
B	-0.134997	B	0.0327594
C	-0.047024	C	-0.059352
D	1.5370699	D	1.5821536
E	1.5214034	E	1.5792014
A*B	-0.015726	F	-0.015648
A*C	-0.020587	A*B	-0.01704
B*C	0.0067479	A*C	0.0183019
A*D	0.0027028	B*C	-0.005857
B*D	-0.023491	A*D	-0.063305
C*D	-0.01779	B*D	0.014694
A*E	0.0066554	C*D	-0.035919
B*E	-0.01104	A*E	-0.052929
C*E	-0.014589	B*E	0.0105379
D*E	-0.022106	C*E	-0.032328
A*A	0.0005425	D*E	0.0475127
B*B	0.0626414	A*F	0.0055047
C*C	-0.029485	B*F	-0.003985
D*D	-0.040775	C*F	0.0048729
E*E	-0.10486	D*F	-0.002191
		E*F	-0.004579
		A*A	0.0474232
		B*B	5.57E-05
		C*C	-0.023057
		D*D	0.0086827
		E*E	-0.00983
		F*F	-0.000337

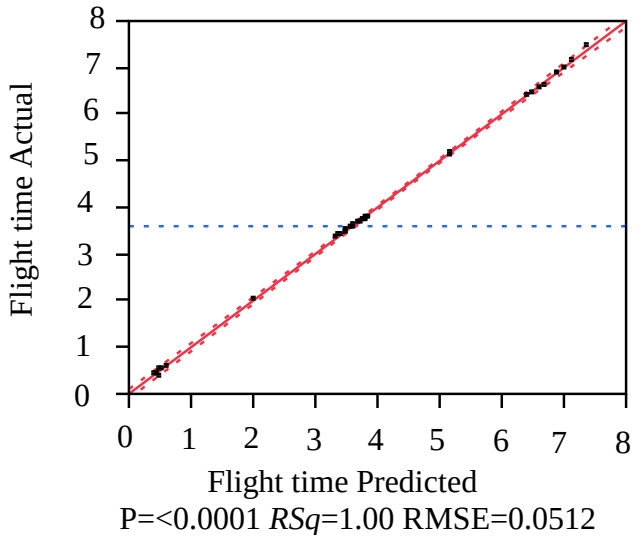

Fig. 2-5 Actual by Predicted plot generated in JMP® for the face-centered design for the slave signal. The red diagonal line is the line of fit, the dashed horizontal blue line is set at the mean of the simulated flight times, and the dashed red curves are the confidence bands for the mean [Jmp-16].

2.2. Validating the Model

The models obtained are validated only for the master signal, since the same procedure was followed to obtain the models for the slave signal.

Starting with the rotatable design, it is validated with the factor ranges at a distance no larger than ±1, since the manufacturing process assures master_corner, slave_corner, and the Zo of the transmission lines will stay within their high and low values, and will never go beyond that range. The design levels and values of the factors for the validation of the model are shown in TABLE XIX. Two intermediate levels (-0.5 and 0.5) were added for master_corner, slave_corner, and the length of the transmission lines, to evaluate the model in other points that were not included in the simulation runs for the design in TABLE XII.

All possible combinations for factors and levels in TABLE XIX result in 1875 runs. To validate the model, all the combinations are input into the quadratic regression model in (2-4) with the help of Matlab scripts, and flight times are measured from the 1875 simulated runs. The absolute difference between the measured and the estimated flight times is presented as the error of the model. A 15% error is considered acceptable for this model. For better visualization, the 1875 combinations are organized in matrix form and the error of the model is presented as a contour plot in Fig. 2-6, with the levels of Zo of board routing, length of L1 and L2 in the y-axis (shown in TABLE XX), and the levels for master_corner and slave_corner in the x-axis (shown in TABLE XXI). The contour plot shows no error is greater than 15% for the CCD with $\alpha=2$.

However, with this design there is a limitation in the allowable range for the lengths of L1 and L2, making the total length of the interconnection allowed from 5.51 in to 16.49 in.

TABLE XIX
LEVELS FOR ROTATABLE MODEL VALIDATION

Factor	Symbol	Value at -1	Value at -0.5	Value at 0	Value at +0.5	Value at +1
slave_corner	A	3.135V	3.2175V	3.3V	3.3825V	3.465V
master_corner	B	3.135V	3.2175V	3.3V	3.3825V	3.465V
Zo of board routing	C	46ohm	-	50ohm	-	54ohm
Length of L1	D	2.005in	3.7525in	4in	4.9975in	5.995in
Length of L2	E	3.505in	5.2525in	7in	8.7475in	10.495in

TABLE XX
Y-AXIS COMBINATIONS FOR CONTOUR PLOTS

Label	Zo	L1	L2
Cn1	-1	-1	-1
Cn2	-1	-1	-0.5
Cn3	-1	-1	0
Cn4	-1	-1	0.5
Cn5	-1	-1	1
Cn6	-1	-0.5	-1
Cn7	-1	-0.5	-0.5
Cn8	-1	-0.5	0
Cn9	-1	-0.5	0.5
Cn10	-1	-0.5	1
Cn11	-1	0	-1
Cn12	-1	0	-0.5
Cn13	-1	0	0
Cn14	-1	0	0.5
Cn15	-1	0	1
Cn16	-1	0.5	-1
Cn17	-1	0.5	-0.5
Cn18	-1	0.5	0
Cn19	-1	0.5	0.5
Cn20	-1	0.5	1
Cn21	-1	1	-1
Cn22	-1	1	-0.5
Cn23	-1	1	0
Cn24	-1	1	0.5
Cn25	-1	1	1
Cn26	0	-1	-1
Cn27	0	-1	-0.5
Cn28	0	-1	0
Cn29	0	-1	0.5
Cn30	0	-1	1
Cn31	0	-0.5	-1
Cn32	0	-0.5	-0.5
Cn33	0	-0.5	0
Cn34	0	-0.5	0.5
Cn35	0	-0.5	1
Cn36	0	0	-1
Cn37	0	0	-0.5
Cn38	0	0	0

Label	Zo	L1	L2
Cn39	0	0	0.5
Cn40	0	0	1
Cn41	0	0.5	-1
Cn42	0	0.5	-0.5
Cn43	0	0.5	0
Cn44	0	0.5	0.5
Cn45	0	0.5	1
Cn46	0	1	-1
Cn47	0	1	-0.5
Cn48	0	1	0
Cn49	0	1	0.5
Cn50	0	1	1
Cn51	1	-1	-1
Cn52	1	-1	-0.5
Cn53	1	-1	0
Cn54	1	-1	0.5
Cn55	1	-1	1
Cn56	1	-0.5	-1
Cn57	1	-0.5	-0.5
Cn58	1	-0.5	0
Cn59	1	-0.5	0.5
Cn60	1	-0.5	1
Cn61	1	0	-1
Cn62	1	0	-0.5
Cn63	1	0	0
Cn64	1	0	0.5
Cn65	1	0	1
Cn66	1	0.5	-1
Cn67	1	0.5	-0.5
Cn68	1	0.5	0
Cn69	1	0.5	0.5
Cn70	1	0.5	1
Cn71	1	1	-1
Cn72	1	1	-0.5
Cn73	1	1	0
Cn74	1	1	0.5
Cn75	1	1	1

TABLE XXI
X-AXIS COMBINATIONS FOR CONTOUR PLOTS

Label	slave	master
Cm1	-1	-1
Cm2	-0.5	-1
Cm3	0	-1
Cm4	0.5	-1
Cm5	1	-1
Cm6	-1	-0.5
Cm7	-0.5	-0.5
Cm8	0	-0.5
Cm9	0.5	-0.5
Cm10	1	-0.5
Cm11	-1	0
Cm12	-0.5	0
Cm13	0	0
Cm14	0.5	0
Cm15	1	0
Cm16	-1	0.5
Cm17	-0.5	0.5
Cm18	0	0.5
Cm19	0.5	0.5
Cm20	1	0.5
Cm21	-1	1
Cm22	-0.5	1
Cm23	0	1
Cm24	0.5	1
Cm25	1	1

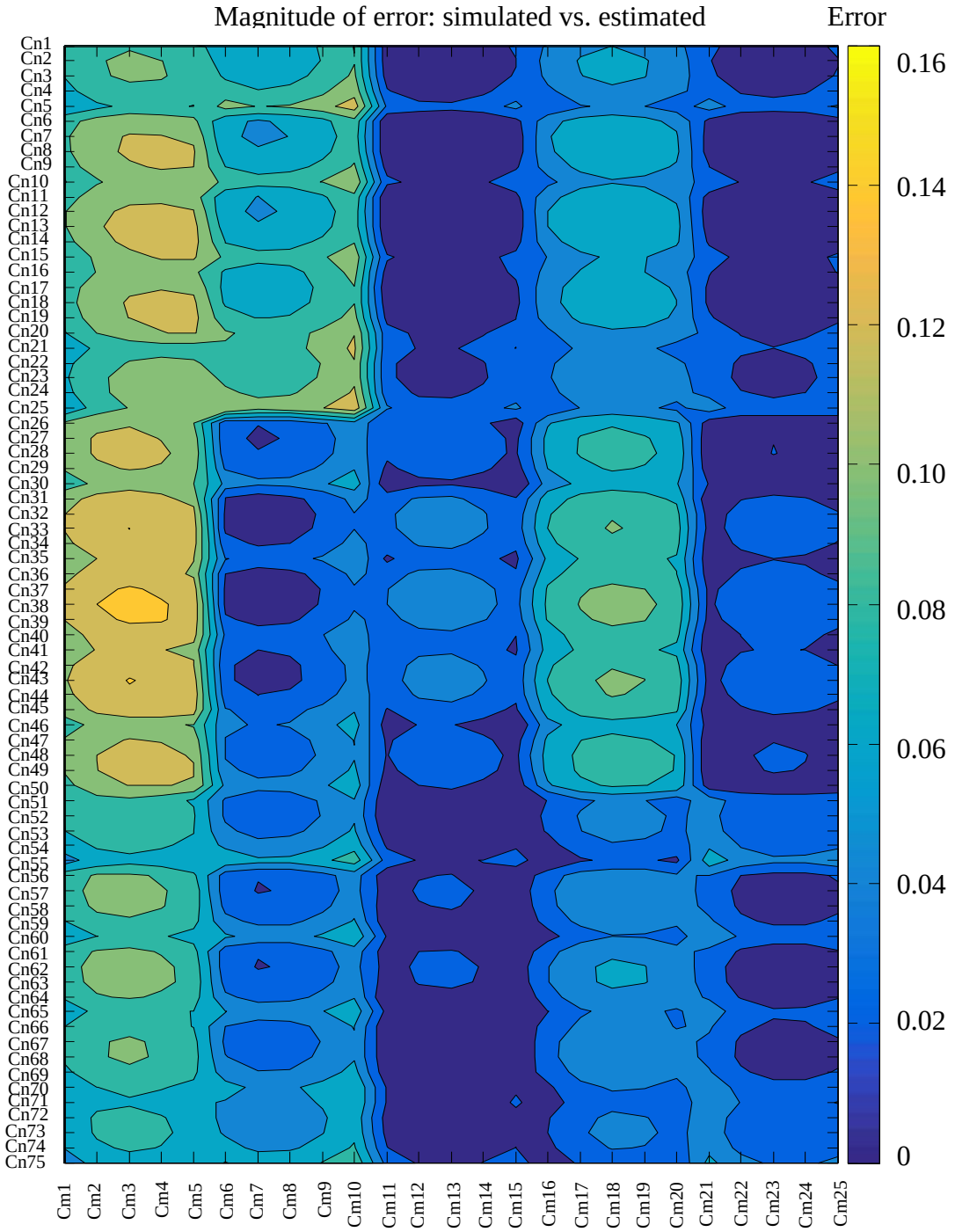

Fig. 2-6 Contour plot of the error of the quadratic regression model for the rotatable CCD experiment using $\alpha = 2$. Cn## correspond to the combinations of the levels of Zo of the board routing, lengths L1 and L2. Cm## are the combinations of the levels for master_corner and slave_corner.

For the face-centered model two intermediate levels (-0.5 and 0.5) are added for the design levels and values of the factors are shown in TABLE XXII. All possible combinations for factor and levels in TABLE XXII result in 1875 runs, and the same procedure is followed as with the rotatable design with α=2. A 15% error is considered acceptable for this model. The 1875 combinations are organized in matrix form and the error of the model is presented as a contour plot in Fig. 2-7, with the levels of Zo of board routing, length of L1 and L2 in the y-axis (as shown in TABLE XX), and the levels for master_corner and slave_corner in the x-axis (as shown in TABLE XXI). Although this model presents a better fit to the data, it is worse at predicting values than the model with α=2. This can be seen in Fig. 2-7 where there are bright yellow areas that present the largest error. From the 1875 combinations tried in the verification, with α=2 no combination had an error larger than 15%. For the case of α=1, 6 combinations present an error larger than 15%. This means that if there is a need for accuracy of the prediction, the model with α=2 should be used, however, if more range for the lengths of L1 and L2 is required, the model with α=1 can be used in exchange for a bit less accuracy.

TABLE XXII
LEVELS FOR FACE-CENTERED MODEL VALIDATION

Factor	Symbol	Value at -1	Value at -0.5	Value at 0	Value at +0.5	Value at +1
master_corner	A	3.135V	3.2175V	3.3V	3.3825V	3.465V
slave_corner	B	3.135V	3.2175V	3.3V	3.3825V	3.465V
Zo of board routing	C	46ohm	-	50ohm	-	54ohm
Length of L1	D	0.01 in	2.005 in	4 in	5.995 in	7.99 in
Length of L2	E	0.01 in	3.505 in	7 in	10.495 in	13.99 in

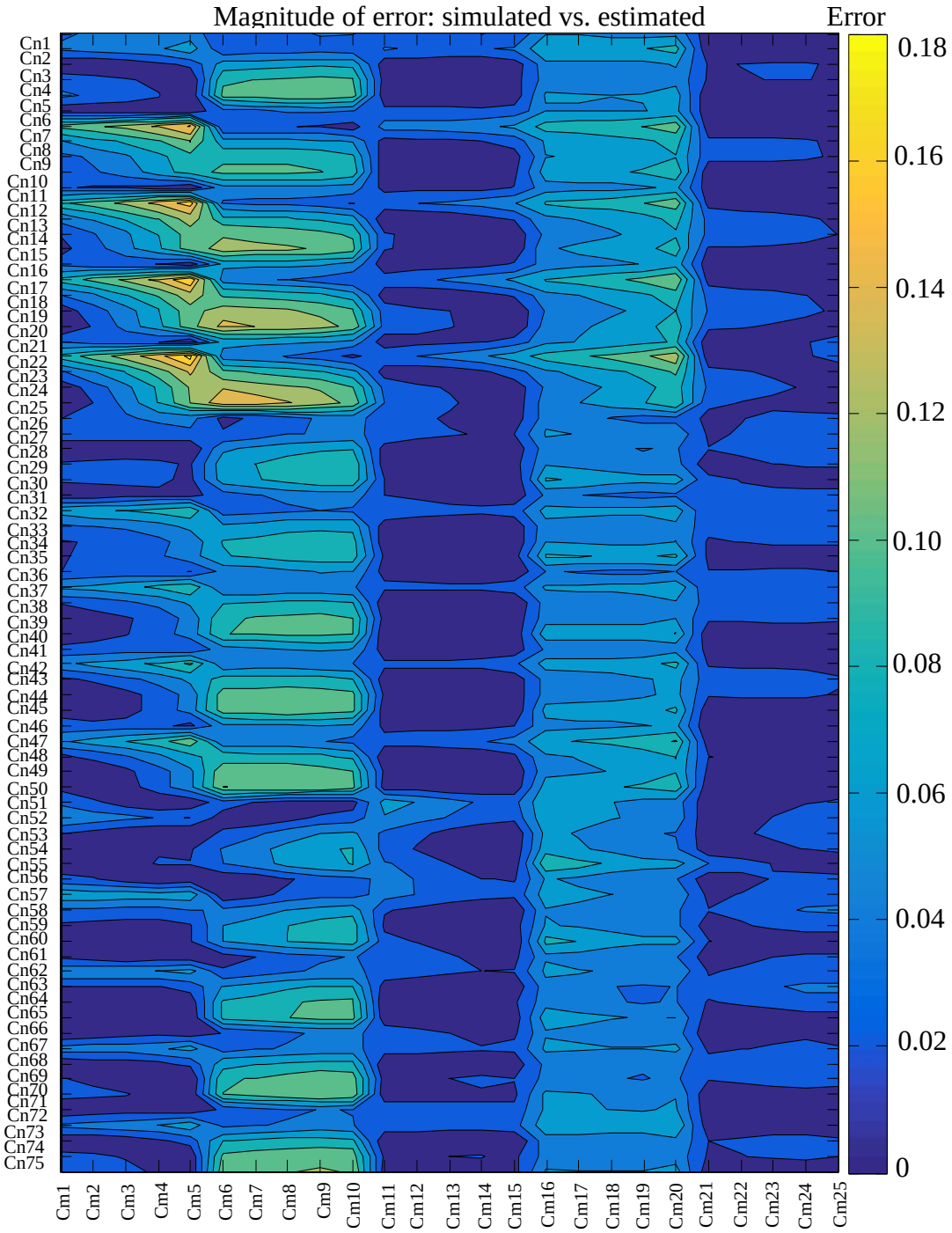

Fig. 2-7 Contour plot of the error of the quadratic regression model for the CCD experiment using $\alpha = 1$. Cn## correspond to the combinations of the levels of Zo of the board routing, lengths L1 and L2. Cm## are the combinations of the levels for master_corner and slave_corner.

2.3. Applying the Model

The circuit in Fig. 1-2 can be used to simulate many different busses, like the Serial Peripheral Interface (SPI) which is one of the miscellaneous I/Os. The SPI is a synchronous data link for serial communication, with a programmable configuration that allows to gluelessly interface one master and one or several slaves. Since SPI is a synchronous bus, it is necessary to perform a timing analysis to comply with setup and hold margins required by both the master and the slave.

The SPI bus consists typically of a clock signal that provides the reference timing to synchronize the data transfer, data lines (2 or 4 uni- or bidirectional depending on the operating mode), and one Chip Select (CS) for each slave [Texas Instruments-12]. SPI can operate in 3 different modes: single mode, where IO0 is called MOSI (Master-Output Slave-Input unidirectional data line), and IO1 is called MISO (Master-Input Slave-Output unidirectional data

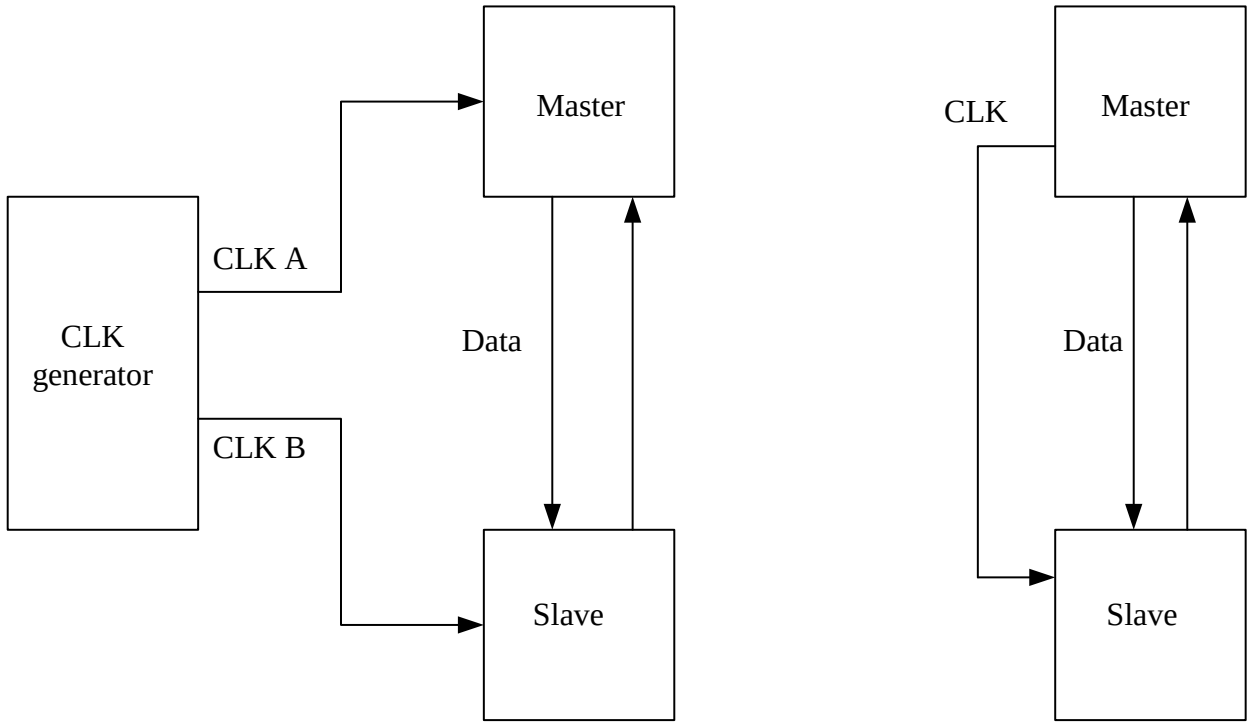

Fig. 2-8 Block diagram of synchronous timing techniques. a) common-clock bus b) source synchronous bus.

line), dual mode, where IO0 and IO1 are bi-directional data lines, and quad mode, where in addition to IO0 and IO1, there are two other bidirectional data lines, IO2 and IO3 [Texas Instruments-12]. No matter the operating mode, the same timing analysis must be applied for this bus.

There are two types of synchronous timing techniques, common-clock and source synchronous. In a common-clock timing scheme, a separate clock generator is used to synchronize the master and the slaves in the bus, as shown in Fig. 2-8 a). In a source synchronous timing scheme, the clock signal is sent from the master instead of a separate source, as shown Fig. 2-8 b) [Hall-00].

For a WRITE operation (data transfer from the master to the slave), the SPI bus is typically programmed so that data is sent out of the master on the first rising edge of the clock, and latched to the input of the slave device at the immediate next falling edge of the clock. This transaction follows a source synchronous timing scheme. On a rising edge of the Clock signal, the master outputs a data bit after a small delay called T_{co_master}. That data bit needs to arrive at the slave before a determined amount of time (setup time requirement) before the immediate next falling edge of the clock reaches the slave input. The margin in time that the bit will have to comply with that setup time requirement is called the setup time margin, and is the time that the Clock signal stays high (T_{clk_high}), plus the time it takes the falling edge of the Clock signal to arrive at the slave input ($T_{flight\_clock\_master\text{-}to\text{-}slave}$), minus the T_{co_master}, minus the time it takes the data bit to arrive at the slave input ($T_{flight\_data\_master\text{-}to\text{-}slave}$), minus the setup time requirement of the slave (T_{setup_slave}). This process is observed in Fig. 2-9, and translates into the setup time margin equation in (2-10).

The data bit sent from the master is latched to the input of the slave on the falling edge of the Clock signal, and needs to remain stable for a determined amount of time (hold time requirement) after the falling edge of the Clock arrived at the input of the slave. The margin in time that the bit will have to comply with that hold time requirement is the time that the Clock signal stays low (T_{clk_low}), plus the T_{co_master}, plus the time it takes the data bit to arrive at the slave input ($T_{flight\_data\_master\text{-}to\text{-}slave}$), minus the time it takes the falling edge of the Clock signal to arrive at input of the slave ($T_{flight\_clk\_master\text{-}to\text{-}slave}$), minus the hold time requirement of the slave (T_{hold_slave}). This process is shown in Fig. 2-10 and gives equation (2-11).

$$T1_{setup\_margin} = T_{clock\_high} + T_{flight\_clock\_master\text{-}to\text{-}slave} - T_{co\_master\_max} - T_{flght\_data\_master\text{-}to\text{-}slave} - T_{setup\_slave} \quad (2\text{-}12)$$

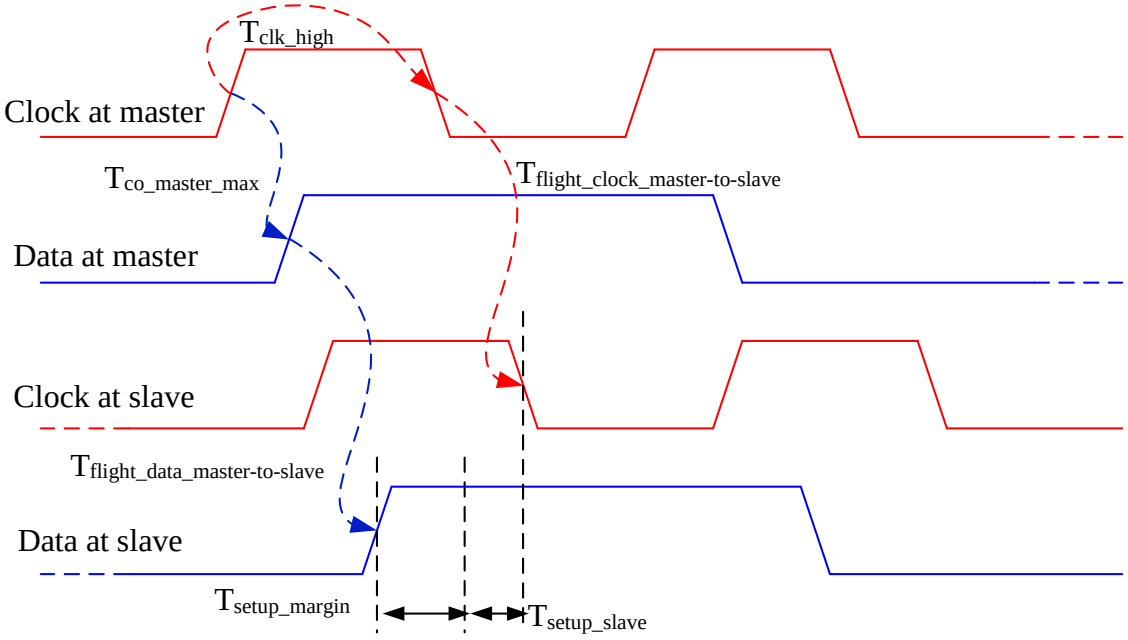

Fig. 2-9 Setup margin derivation for WRITE operation.

$$T1_{hold\_margin} = T_{clk\_low} + T_{flight\_data\_master\text{-}slave} + T_{co\_master\_min} - T_{flight\_clk\_master\text{-}slave} - T_{hold\_slave} \quad (2\text{-}13)$$

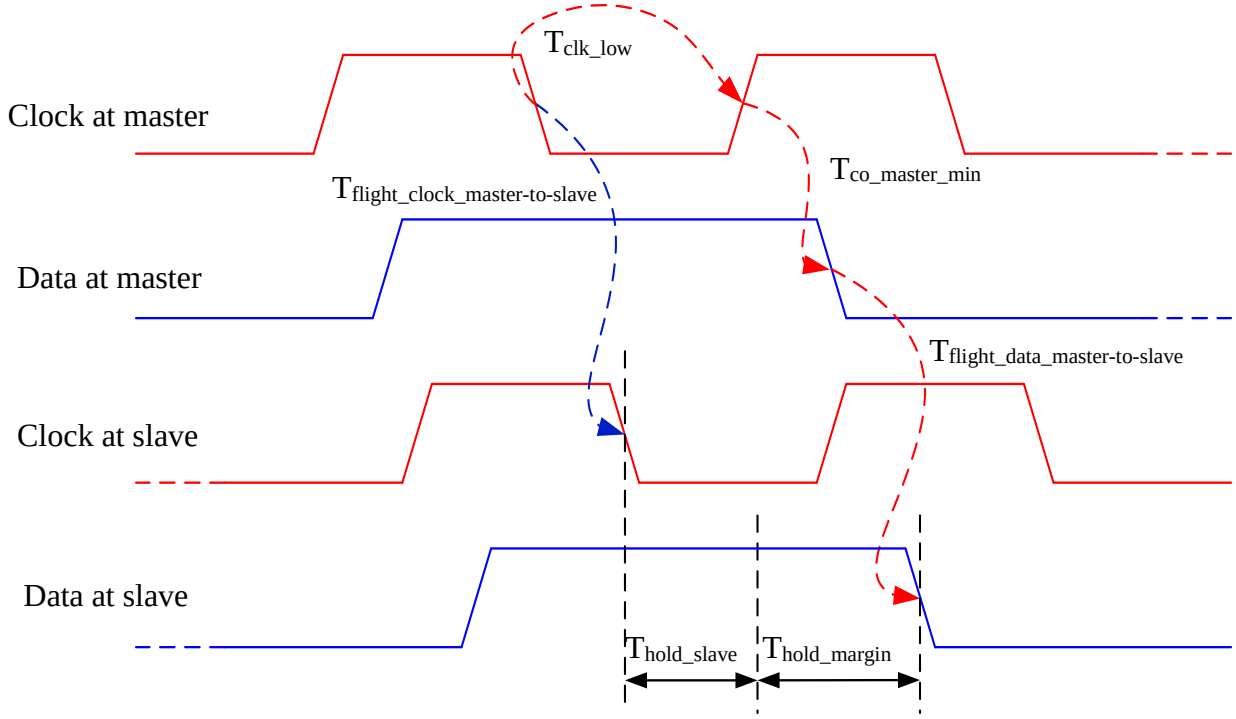

Fig. 2-10 Hold margin derivation for WRITE operation.

For a READ operation (data transfer from the slave back to the master), the SPI bus can be programmed so that data is sent out of the slave device on the rising edge of the Clock signal at the slave, and latched to the input of the master on the next rising edge of the Clock signal. This transaction is somewhat similar to a common-clock scheme since the slave will output a data bit when an external Clock signal reaches its input.

When the rising edge of the Clock signal coming from the master reaches the slave input, the slave outputs a data bit after a small delay called T_{co_slave}. That data bit needs to arrive at the master before a determined amount of time (setup time requirement) before the next rising edge of the clock at the master. The margin in time that the bit will have to comply with that setup time requirement, is the cycle time of the Clock signal (T_{cycle}), minus the time it takes the falling edge of the Clock signal to arrive at the slave input ($T_{flight\_clock\_master\text{-}to\text{-}slave}$), minus the T_{co_slave}, minus the time it takes the data from the slave to arrive at the input of the master ($T_{flight\_data\_slave\text{-}to\text{-}master}$), minus the setup time requirement of the master. This process is observed in Fig. 2-11 and translates into the setup time margin equation in (2-12).

The data bit sent from the slave is latched to the input of the master on the rising edge of the Clock signal, and needs to remain stable for a determined amount of time (hold time requirement) after that rising edge of the Clock signal at the master. The margin in time that the bit will have to comply with that hold time requirement is the time it takes the rising edge of the Clock signal to arrive at the slave input ($T_{flight\_clk\_master\text{-}to\text{-}slave}$), plus the T_{co_slave}, plus the time it takes the data bit to arrive at input of the master ($T_{flight\_data\_slave\text{-}to\text{-}master}$), minus the hold time requirement of the master ($T_{hold\_smaster}$). This process is shown in Fig. 2-12 and gives equation (2-13).

$$T2_{setup\_margin} = T_{cycle} - T_{flight\_clk\_master\text{-}slave} - T_{co\_slave\_max} - T_{flight\_data\_slave\text{-}master} - T_{setup\_master} \quad (2\text{-}14)$$

$$T2_{hold\_margin} = T_{flight\_clk\_master\text{-}slave} + T_{co\_slave\_min} + T_{flight\_data\_slave\text{-}master} - T_{hold\_master} \quad (2\text{-}15)$$

In order to analyze the SPI interface timing requirements using (2-10), (2-11), (2-12), and (2-13), flight times for the clock and data lines are needed.

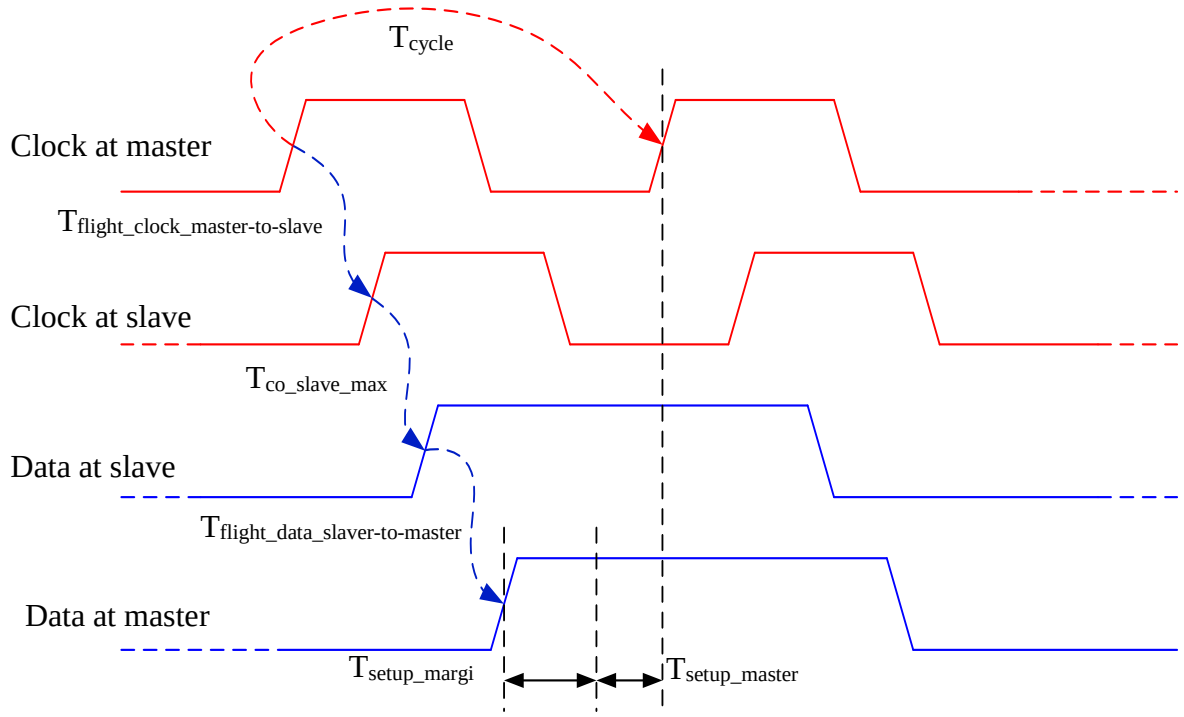

Fig. 2-11 Setup margin derivation for READ operation.

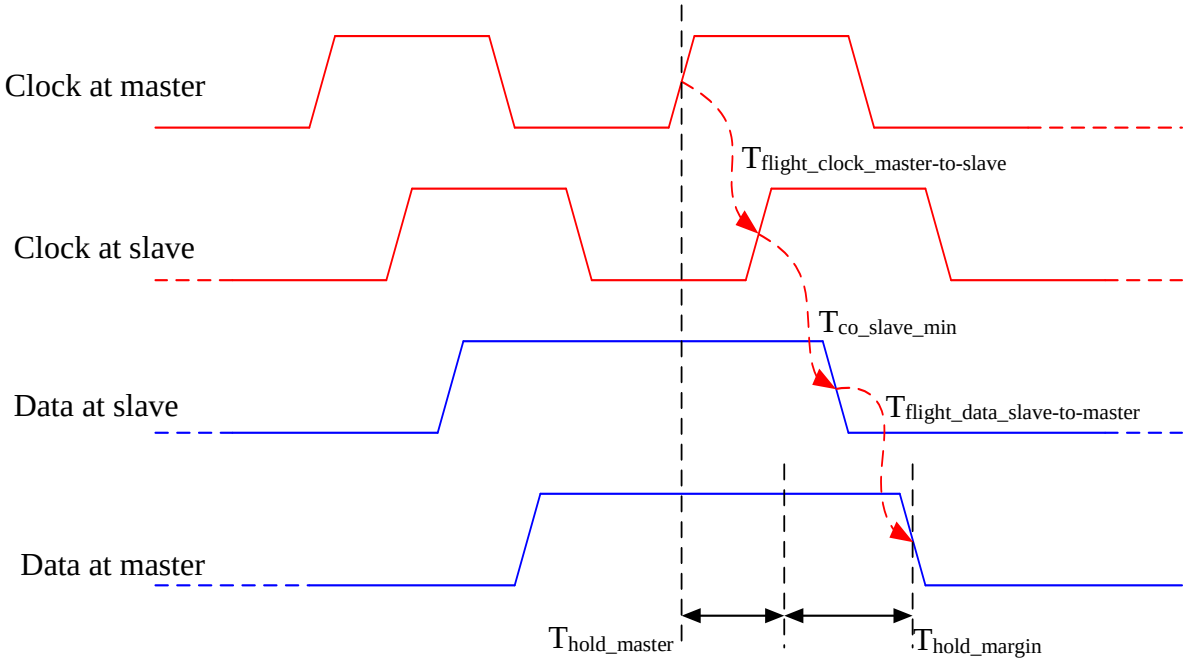

Fig. 2-12 Hold margin derivation for READ operation.

The coefficients in will be used for the regression model of the clock line, as well as the MOSI data line, as the digital signals will follow the same path out of the master buffer, only at a different frequency.

2.4. Conclusions

In this chapter, central composite designs (CCD) were used to fit mathematical models that considered the curvilinear factor effects for the signal coming from the master buffer as well as for the signal coming from the slave buffer. Two types of CCD were compared in terms of their model fit and their ability to make good predictions outside of the experimental region. Both models were validated comparing their results with simulations of the system. The face-centered model was less complex and provided a better model fit but was not as powerful at extrapolating predictions. The rotatable model was good at predicting, but it presented a limitation for the allowable range for the lengths L1 and L2. This makes the face-centered design a better option if more range for the lengths is required, in exchange for a bit less accuracy when extrapolating. These quadratic regression models were used to represent the CLK, MOSI and MISCO lines of a Serial Peripheral Interface (SPI), in order to be used as the flight time information in a timing margin analysis.

3. Direct Optimization of SPI Interface Using Surrogate Models

In Chapter 2, surrogate models were properly adjusted and validated, which describe the response surfaces modeled for the topology in Fig. 1-2, for clock, MOSI, and MISO lines of the SPI interface. These models can be used to explore the combination of levels of the factors that result in an optimal value of the response. The model should describe at least 70% of the response behavior in terms of R_{adj} for it to be used for optimization purposes [Gutierrez Pulido-12].

The algorithm chosen for an optimization task will depend on the type of problem, the nature of the algorithm, the quality of solutions required, the available computing resources, time limitations, availability of the algorithm for implementation, among others [Zhang-13].

Numerical algorithms for nonlinear optimization can be either gradient-based methods or direct search methods. Examples of gradient-based methods include sequential programming method, augmented Lagrangian method, and the interior point method. Direct search methods include methods such as Nelder-Mead, genetic algorithms, differential evolution, and simulated annealing. Gradient-based methods use first derivatives (gradients) or second derivatives (Hessians), while direct search methods do not make use of derivative information. Though direct search methods tend to converge more slowly, they can be more tolerant to the presence of noise in the function and constraints [Wolfram-16].

3.1. Nelder-Mead Algorithm

The Nelder-Mead simplex algorithm is the most widely used direct search method for solving the unconstrained optimization problem of finding the minimum value of the objective function $f(x)$ [Gao-10]

$$\min_{x} f(x) \tag{3-1}$$

Although it is not a true global optimization algorithm, in practice it tends to work reasonably well for problems that do not have many local minima [Wolfram-16].

3. DIRECT OPTIMIZATION OF SPI INTERFACE USING SURROGATE MODELS

For a function of *n* variables, the algorithm maintains a set of *n*+1 points forming the vertices of a simplex (a generalized triangle in *n*-dimensional space). For simplicity, a simplex in the *n*-dimension space is referred to as *n*-simplex. Therefore, a 1-simplex is a line segment, a 2-simplex is a triangle, a 3-simplex is a tetrahedron, and so on [Zhang-13]. The algorithm is a pattern search that compares function values at the three vertices of a triangle [Mathews-14].

The Nelder-Mead algorithm uses four types of transformations to form a new simplex in each step: reflection away from the worst vertex (the one with the largest function value), shrinkage towards the best vertex (the one with the smallest function value), expansion and contraction that allow the working simplex to change in size and shape [Singer-09].

In [Gavin-16] an easy explanation of the algorithm is given as follows. Consider a simplex of three points [*u*,*v*,*w*] in the $x_1 - x_2$ plane, the triangle connecting them, and the objective function evaluated at the three points, $f(u)$, $f(v)$, and $f(w)$. Point *u* is the best point, point *v* is the next-to-worst point, and point *w* is the worst point.

After constructing the initial *n*-simplex, the next step in the Nelder-Mead algorithm is to evaluate the objective function at the vertices, ranking the objective values and re-ordering the vertices such that

$$f(u) < f(v) < f(w) \tag{3-2}$$

The next step is to reflect the worst point, *w*, through the centroid of the remaining points to obtain the reflected point *r*, and evaluate the objective function $f(r)$ at this new point. Following this, if

$$f(u) < f(r) < f(v) \tag{3-3}$$

then the worst point *w* is replaced with the reflected point *r*, and then the algorithm proceeds to check convergence. Otherwise, if

$$f(r) < f(u) \tag{3-4}$$

then the reflected point *r* is extended further past the average of *u* and *v* to point *e*. The objective function $f(e)$ is evaluated now at the extended point. If the objective value at point *e*, is better than the objective value at point *r*, then the worst point *w* is replaced with the extended point *e* and convergence is checked for. Otherwise, the worst point *w* is replaced with point *r*, and then convergence is checked for.

In the case that

$$f(r) > f(v) \tag{3-5}$$

then a smaller value of the objective function might be found between points *w* and *r*. The algorithm then contracts the worst point *w* to a point *c* between points *w* and *r*, and evaluate $f(c)$. Typical values of *c* are one-quarter (inside contraction c_1) and three-quarters (outside contraction c_0) of the way from *w* to *r*. If

$$\min[\, f(c_1), f(c_0) < f(v)] \tag{3-6}$$

then the worst point *w* is replaced with the better contraction point, and check for convergence. Otherwise, the simplex is shrunk into the best point, *u*, and check for convergence.

If convergence is not yet reached, the next iteration begins sorting the vertices of the simplex again, unless the number of function evaluations has exceeded a specific limit, in which case the algorithm is terminated.

Convergence is reached if the parameter differences between adjacent vertices is less than ε_p times the parameter average of adjacent vertices

$$2\max\left|\frac{[u,v]-[v,w]}{[u,v]+[v,w]}\right| < \varepsilon_p \tag{3-7}$$

and the objective function at all vertices is within ε_f times the best objective value.

$$2\max\left|\frac{f(u)-[\, f(v), f(w)]}{f(u)+10^{-9}}\right| < \varepsilon_f \tag{3-8}$$

The Nelder-Mead algorithm can be extended to constrained minimization problems by adding a penalty function. This is accomplished by adding a term to the objective function that highly increases the objective value in case of constraint violation

$$\min_x f(x) + cP(x) \tag{3-9}$$

where $f(x)$ is the objective function to minimize, $P(x)$ is the penalty function, and *c* is the penalty parameter [Freund-14].

FMINSEARCH is the Matlab implementation of the Nelder-Mead method; it finds the minimum of the objective function, a scalar function of several variables. It starts at the point x_0

(initial seed value selected) and returns a value x^* that is the local minimizer of the objective function,

$$x^* = \arg\min_x f(x) \tag{3-10}$$

The algorithm forms the initial simplex by choosing the starting point x_0 as one of the initial simplex vertices. The remaining *n* vertices are generated using $x_0 + \tau_i e_i$, where e_i is the unit vector in the *i*th coordinate, and τ_i is chosen as in equation (3-11) [Gao-10]

$$\tau_i = \begin{cases} 0.05 & if\,(x_0)_i \neq 0 \\ 0.00025 & if\,(x_0)_i = 0 \end{cases} \tag{3-11}$$

FMINSEARCH uses TolFun, TolX, MaxIter, and MaxFunEvals parameters to terminate the algorithm when one of the following criteria is met [Gao-10]:

(T1) $\max_{2\le i\le n+1} |f_i - f_l| \le TolFun$ and $\max_{2\le i\le n+1} \|x_i - x_l\|_\infty \le TolX$

(T2) The number of iterations has exceeded MaxIter

(T3) The number of function evaluations exceeds MaxFunEvals

3.2. Implementing the Algorithm

The SPI interface is a synchronous data link, therefore a timing analysis needs to be done to determine the possible lengths for the clock and data lines. This timing analysis consists in calculating the margin equations (2-10), (2-11), (2-12) and (2-13), using flight time information from calculations or simulation.

Using the coefficients in TABLE XVII and TABLE XVIII to calculate flight times for the timing margins in (2-10) to (2-13), an optimization task is done in order to find the maximum lengths of L1 and L2 for the clock and data lines while maintaining the four timing margins equal to, or larger than zero. The objective function for the optimization task is that all four timing margins must be equal to or more than zero.

Timing margin $T2_{hold\_margin}$ from equation (2-13) will remain positive if the following is true:

1. $T_{co\_slave\_min} > 0$ or $T_{flight\_clk\_master\text{-}slave} + T_{flight\_data\_slave\text{-}master} > T_{co\_slave\_min}$

2. $T_{flight\_clk\_master\text{-}slave} + T_{co\_slave\_min} + T_{flight\_data\_slave\text{-}master} \geq T_{hold\_master}$

$T2_{hold\_margin}$ will be left out of the objective function as it will be assumed that the above points will be met.

The objective function can be further simplified if the total length of the clock line is the same as the total length of each data line, then timing margin $T1_{setup\_margin}$ from equation (2-10) and timing margin $T1_{hold\_margin}$ from equation (2-11) become independent of length, since the clock line flight time and the data lines flight times cancel each other out. To enable this, an upper-bound constraint will be added to the objective function, where each data line length is allowed to be unmatched to the clock line length by no more than 250 mils.

The objective function can then involve only $T2_{setup\_margin}$, which is the only timing margin left that could become negative as the lengths of L1 and L2 become maximized. Thus, the objective function is written as (3-12)

$$f(x) = \begin{cases} \dfrac{T2_{setup\_margin}}{\varepsilon_1} - 1 & if \quad T2_{setup\_margin} > 0 \\ 1 - \dfrac{T2_{setup\_margin}}{\varepsilon_1} & if \quad T2_{setup\_margin} < 0 \end{cases} \tag{3-12}$$

where $T2_{setup\_margin}$ is the setup margin calculated using (2-12), and ε_1 is a very small positive number, 1e-4. $T2_{setup\_margin}$ 8.4557 will become negative if the transmission lines are too long. The objective function looks for the smallest value of $T2_{setup\_margin}$ without it becoming negative.

Since Nelder-Mead method will be used for the optimization task, a penalty function must be introduced in order to subject the objective function to a constraint. The penalty functions to be used are defined by

$$P_1(x) = \left[\frac{\left| length_{clk} - length_{MOSI} \right|}{x^{ub}} \right] - 1 \tag{3-13}$$

$$P_2(x) = \left[\frac{\left| length_{clk} - length_{MISO} \right|}{x^{ub}} \right] - 1 \tag{3-14}$$

where $length_{clk}$ is the total length of the clock line, $length_{MOSI}$ and $length_{MISO}$ are the total lengths of the data lines, and x^{ub} is the upper-bound constraint of 250 mils.

3.3. Optimization Results Using Fminsearch

Six optimization runs were performed using different seed values for the value of L1 for clock and data lines, for both the rotatable (α=2 for clock and MOSI lines, and α=2.378 for MISO line) and the face-centered (α=2 for clock, MOSI and MISO lines) regression models. The value of L2 of all three lines was maintained fixed to simplify the optimization efforts, as there are many combinations of L1 and L2 values that will result in an optimized objective function. The optimized length values are shown in TABLE XXIII and TABLE XXIV. The four optimized timing margins are shown for each run, as well as the value of the objective function $f(x)$ at the optimized values (feval), the number of iterations (iter) and number of function evaluations (funcCount) taken.

For both designs, an average of the optimized lengths was calculated and a SPICE simulation was executed using those values. Flight times were measured as explained in Chapter 2, and compared with the flight times estimated with the regression models.

TABLE XXIII
OPTIMIZATION RESULTS FOR THE ROTATABLE CCD EXPERIMENT FOR THE CLOCK, MOSI AND MISO LINES

		Run 1		Run 2		Run 3		Units
		Seed value	Optimized value	Seed value	Optimized value	Seed value	Optimized value	
Clock	L1	9	19.313	18	19.310	17	19.385	in
	L2 fixed	3	--	3	--	3	--	in
MOSI	L1	9	19.311	18	19.314	18	19.525	in
	L2 fixed	3	--	3	--	3	--	in
MISO	L1	9	19.311	50	19.314	18	19.240	in
	L2 fixed	3	--	3	--	3	--	in
$T1_{setup\_margin\_optim}$		0.600	0.600	0.600	0.599	0.404	0.573	ns
$T1_{hold\_margin\_optim}$		4.800	4.800	4.800	4.801	4.996	4.828	ns
$T2_{setup\_margin\_optim}$		3.970	6.26E-07	-6.904	1.92E-06	0.717	5.70E-05	ns
$T2_{hold\_margin\_optim}$		8.859	12.830	19.734	12.830	12.113	12.830	ns
feval		-0.990		-0.981		-0.417		
iter/funcCount		207 / 383		132 / 243		103 / 192		

		Run 4		Run 5		Run 6		Units
		Seed value	Optimized value	Seed value	Optimized value	Seed value	Optimized value	
Clock	L1	19	19.371	22	19.2348	14	19.267	in
	L2 fixed	3	--	3	--	3	--	in
MOSI	L1	19	19.490	22	19.0931	22	19.351	in
	L2 fixed	3	--	3	--	3	--	in
MISO	L1	22	19.253	40	19.3870	18	19.3558	in
	L2 fixed	3	--	3	--	3	--	in
$T1_{setup\_margin\_optim}$		0.600	0.504	0.600	0.628	-0.973	0.583	ns
$T1_{hold\_margin\_optim}$		4.800	4.896	4.800	4.772	6.373	4.816	ns
$T2_{setup\_margin\_optim}$		-0.487	3.291E-05	-5.156	4.513E-10	1.302	1.328E-05	ns
$T2_{hold\_margin\_optim}$		13.318	12.830	17.976	12.830	11.528	12.830	ns
feval		-0.528		-0.3914		-0.644		
iter/funcCount		315 / 582		114 / 207		136 / 255		

TABLE XXIV
OPTIMIZATION RESULTS FOR THE FACE-CENTERED CCD EXPERIMENT FOR THE CLOCK, MOSI AND MISO LINES

		Run 1		Run 2		Run 3		Units
		Seed value	Optimized value	Seed value	Optimized value	Seed value	Optimized value	
Clock	L1	12	20.001	18	20.019	18	19.730	in
	L2 fixed	3	--	3	--	3	--	in
MOSI	L1	12	19.899	18	20.806	18	19.101	in
	L2 fixed	3	--	3	--	3	--	in
MISO	L1	12	20.105	42	20.089	17	20.0353	in
	L2 fixed	3	--	3	--	3	--	in
$T1_{setup\_margin\_optim}$		0.600	0.617	0.600	0.466	0.600	0.706	ns
$T1_{hold\_margin\_optim}$		4.800	4.783	4.800	4.932	4.800	4.694	ns
$T2_{setup\_margin\_optim}$		2.890	3.84E-05	-3.778	1.556E-05	0.917	6.465E-05	ns
$T2_{hold\_margin\_optim}$		9.940	12.830	16.608	12.830	11.913	12.830	ns
feval		-0.582		-0.518		-0.697		
iter/funcCount		157 / 389		238 / 442		233 / 435		

		Run 4		Run 5		Run 6		Units
		Seed value	Optimized value	Seed value	Optimized value	Seed value	Optimized value	
Clock	L1	25	20.084	14	20.054	18	19.3156	in
	L2 fixed	3	--	3	--	3	--	in
MOSI	L1	25	20.082	15	20.055	19	19.7486	in
	L2 fixed	3	--	3	--	3	--	in
MISO	L1	19	21.085	25	20.057	22	20.1518	in
	L2 fixed	2	--	3	--	3	3	in
$T1_{setup\_margin\_optim}$		0.600	0.6002	0.424	0.600	0.428	0.569	ns
$T1_{hold\_margin\_optim}$		4.800	4.7998	4.976	4.800	4.971	4.830	ns
$T2_{setup\_margin\_optim}$		-0.629	1.428E-06	0.128	2.023E-6	-0.0101	4.534E-05	ns
$T2_{hold\_margin\_optim}$		13.459	12.8300	12.702	12.830	12.840	12.830	ns
feval		-0.994		-0.9798		-0.2374		
iter/funcCount		278 / 522		140 / 246		100 / 187		

TABLE XXVI and TABLE XXV show the error between the simulated and estimated flight times and timing margins for the optimized lengths. For both the rotatable and face-centered designs, the estimated optimal flight time for the MISO line was more accurate than the estimated optimal ones for the Clock and MOSI lines. This could be due to the fact that for the MISO regression model six variables were used, rather than only five for the Clock and MOSI regression models. All optimization runs gave an optimized $T2_{setup\_margin\_optim}$ timing margin in the order of femtoseconds or less, as was expected when maximizing L1 and L2 lengths. An upper bound restriction was added to the objective function to ensure proper length matching between Clock and data lines, thus $T1_{setup\_margin\_optim}$ and $T1_{hold\_margin\_optim}$ have minimum error compared to $T2_{setup\_margin\_optim}$ and $T2_{hold\_margin\_optim}$.

TABLE XXV
COMPARISON BETWEEN SIMULATED AND ESTIMATED FLIGHT TIMES AND TIMING MARGINS FOR THE FACE-CENTERED EXPERIMENT FOR THE CLOCK, MOSI AND MISO LINES

	L1 (optimized average)	L2 (fixed)	Estimated Flight time	Simulated Flight time	Error	Units
Clock	20.046	3	4.648	4.776	0.129	ns
MOSI	20.004	3	4.641	4.769	0.128	ns
MISO	20.073	3	4.684	4.679	0.005	ns

	Estimated Margin	Simulated Margin	Error	Units
$T1_{setup\_margin\_optim}$	0.607	0.608	0.001	ns
$T1_{hold\_margin\_optim}$	4.793	4.792	0.001	ns
$T2_{setup\_margin\_optim}$	-0.002	-0.125	0.124	ns
$T2_{hold\_margin\_optim}$	0.832	0.955	0.124	ns

TABLE XXVI
SIMULATED AND ESTIMATED FLIGHT TIMES COMPARISON AND TIMING MARGINS FOR THE ROTATABLE EXPERIMENT FOR THE CLOCK, MOSI AND MISO LINES

	L1 (optimized average)	L2 (fixed)	Estimated Flight time	Simulated Flight time	Error	Units
Clock	19.320	3	4.524	4.637	0.113	ns
MOSI	19.369	3	4.533	4.647	0.115	ns
MISO	19.449	3	4.568	4.567	0.001	ns

	Estimated Margin	Simulated Margin	Error	Units
$T1_{setup\_margin\_optim}$	0.592	0.590	0.002	ns
$T1_{hold\_margin\_optim}$	4.808	4.810	0.002	ns
$T2_{setup\_margin\_optim}$	0.238	0.125	0.112	ns
$T2_{hold\_margin\_optim}$	0.5924	0.705	0.112	ns

3.4. Conclusions

In this chapter Nelder-Mead optimization tasks with an added penalty function were performed to maximize the lengths of the CLK, MOSI and MISO lines of the SPI bus described in Chapter 2, while maintaining the timing margins equal to or larger than zero. Rotatable and face-centered designs were used in the optimization tasks. The optimal values were then validated in SPICE simulations. The setup and hold margins for a WRITE operation had minimum error compared to the margins for a READ operation due to the length matching constraint added with the penalty function that makes the timing margins for a WRITE operation practically insensitive to the lengths of the transmission lines. All optimization runs gave an optimized setup margin for the READ operation in the order of femtoseconds or less, as was expected when maximizing L1 and L2 lengths. For both the rotatable and face-centered designs, the estimated optimal flight time for the MISO line was more accurate than the estimated optimal ones for the Clock and MOSI lines, this may be due to the fact that the MISO regression model considered six factors while the Clock and MOSI regression models considered only five.

Conclusions

In this work, surrogate models were obtained to model the flight times of a point-to-point single-ended interconnect, in order to simplify optimization tasks when the models were used to represent a single-ended interface. To decide which factors were to be included in the models, screening experiments were done for both the signal coming out of the master buffer, and the signal coming back from the slave buffer. From the five uncontrollable factors chosen to be investigated, three were concluded to have active effects on the flight time of the master signal. i.e., the operating conditions of both buffers and the characteristic impedance of the PCB transmission lines. These three factors were also determined to have active effects on the flight time of the slave signal, along with the characteristic impedance of the package transmission lines.

The screening experiments only provided direct additive and interaction effects. In order to include curvilinear effects in the surrogate models, central composite designs (CCD) were used. Two types of CCD were compared in terms of their model fit and their ability to make good predictions outside of the experimental region. Both models were validated comparing their results with simulations of the system. The face-centered design resulted in a better option if more range for the lengths is required, but was not as powerful as the rotatable model at extrapolating predictions.

Using the surrogate models obtained (rotatable and face-centered), Nelder-Mead optimization tasks with an added penalty function were run to maximize the allowable lengths of the transmission lines of the SPI bus, while maintaining the timing margins equal to or larger than zero. The optimal values found were then validated using SPICE simulations. The timing margins for a WRITE operation were made practically insensitive to the lengths of the transmission lines with the length matching constraint added with the penalty function, making the error between the surrogate model margins and the simulated margins minimum. All optimization runs gave an optimized setup margin for the READ operation in the order of femtoseconds or less, as was expected when maximizing the lengths of the transmission lines. For both the rotatable and face-centered designs, the estimated optimal flight time for the MISO line was more accurate than the estimated optimal ones for the CLK and MOSI lines, this may be due to the fact that the MISO

regression model considered six factors while the CLK and MOSI regression models considered only five.

Future Work

The methodology proposed in this thesis for obtaining a surrogate model of a single-ended interface to be used in optimization tasks can be taken to further interesting directions. Firstly, the methodology presented was applied only to a simple point-to-point topology. The same approach could be taken with more complex topologies to evaluate if the results in this case are acceptable.

Following from the research presented in Chapter 2 to obtain surrogate models, 3rd order effects could be added to the regression models, or different types of design of experiments, such as Taguchi designs, could be explored.

Finally, gradient-based methods or other direct search optimization methods such as genetic algorithms, could be explored and compared to choose the best one for the point-to-point topology proposed, or to more complex topologies.

Bibliography

[Yelten-12] Yelten, M. B. et al. "Demystifying Surrogate Modeling For Circuits And Systems". IEEE Circuits Syst. Mag. 12.1 (2012): 45-63. Web.

[Savant-98] C. J. Savant, M. S. Rodent and G. L. Carpenter, *Diseño Electrónico*, Mexico: Addison Wesley Longman de Mexico, 1998

[Montgomery-13] D. C. Montgomery, *Design and Analysis of Experiments*, 8th ed., Hoboken, NJ: John Wiley & Sons Inc., 2013.

[Casamayor-04] M. Casamayor, "A First Approach to IBIS Models:What They Are and How They Are Generated," Analog Devices, Inc., Norwood, MA, 2004.

[Li-06] X. Li, N. Sudarsanam and D. D. Frey, "Regularities in data from factorial experiments," *Complexity*, vol. 11, no. 5, pp. 32-45, 2006

[Daniel-59] C. Daniel, "Use of Half-Normal Plots in Interpreting Factorial Two-Level Experiments," *Technometrics*, vol. 1, no. 4, p. 311, 1959.

[Lenth-89] R. Lenth, "Quick and Easy Analysis of Unreplicated Factorials," *Technometrics*, vol. 31, no. 4, p. 469, 1989.

[Mason-03] R. Mason, R. Gunst and J. Hess, *Statistical design and analysis of experiments*, New York: J. Wiley, 2003.

[Box-05] G. Box, J. Hunter and W. Hunter, *Statistics for experimenters*, Hoboken, N.J: Wiley-Interscience, 2005.

[Support.minitab-15] Support.minitab.com, "What is a design generator? - Minitab," Minitab Inc., 2015. [Online]. Available: http://support.minitab.com/en-us/minitab/17/topic-library/modeling-statistics/doe/factorial-designs/what-is-a-design-generator/. [Accessed 30 June 2015]..

[Balasubramaniam-01] S. Balasubramaniam, R. Ammar, E. Cox, S. Blozis and J. M. Soltero, "Basic Design Considerations for Backplanes," Texas Instruments Incorporated, Dallas, Texas, 2001.

[Dodge-08] Y. Dodge, *The concise encyclopedia of statistics*, New York: Springer, 2008.

[NIST/SEMATECH-15]"1.3.5.18. Yates Algorithm," Itl.nist.gov, 2015. [Online]. Available: http://www.itl.nist.gov/div898/handbook/eda/section3/eda35i.htm. [Accessed 14 July 2015].

[Hall-00] S. Hall, G. Hall and J. McCall, High speed digital system design, New York: Wiley, 2000.

[Verseput-00] R. Verseput, "Digging Into DOE: Selecting the right central composite design for response surface methodology applications," QCI International, 2000. [Online]. Available: http://www.qualitydigest.com/june01/html/doe.html. [Accessed 11 May 2015].

[Myers-02] R. Myers and D. Montgomery, *Response surface methodology*, New York: J. Wiley, 2002.

[Kuehl-01] R. Kuehl, Diseño de experimentos, Mexico, D.F.: Thomson Learning, 2001.

[Grace-Martin-15] K. Grace-Martin, "Assessing the Fit of Regression Models," Theanalysisfactor.com, 2015. [Online]. Available: http://www.theanalysisfactor.com/assessing-the-fit-of-regression-models. [Accessed 8 July 2015].

[Allen-10] T. Allen, *Introduction to Engineering Statistics and Lean Sigma*, London: Springer, 2010.

[Jmp-16] "Row Diagnostics". Jmp.com. N.p., 2016. Web. 20 July 2016.

[Texas Instruments-12] "KeyStone Architecture Literature Serial Peripheral Interface (SPI)," Texas Instruments, Dallas, 2012.

[Gutierrez Pulido-12] H. Gutierrez Pulido y R. D. L. Vara Salazar, *Análisis y diseño de experimentos*, Mexico: McGraw-Hill Interamericana, 2012.

[Zhang-13] Q.-J. Zhang, X.-S. Yang and S. Koziel, *Simulation-driven Design Optimization and Modeling for Microwave Engineering*, London: Imperial College Press, 2013.

[Wolfram-16] "Numerical Nonlinear Global Optimization—Wolfram Language Documentation," Reference.wolfram.com, 2016. [Online]. Available: http://reference.wolfram.com/language/tutorial/ConstrainedOptimizationGlobalNumerical.html#434989722. [Accessed 14 January 2016].

[Gao-10] F. Gao and L. Han, "Implementing the Nelder-Mead simplex algorithm with adaptive parameters," *Computational Optimization and Applications*, vol. 51, no. 1, pp. 259-277, 04 May 2010.

[Mathews-14] J. Mathews and K. Fink, *Numerical methods using MATLAB*, Upper Saddle River, N.J.: Pearson, 2014.

[Singer-09] S. Singer and J. Nelder, "Nelder-Mead algorithm," Scholarpedia, vol. 4, no. 7, p. 2928, 2009.

[Gavin-16] H. Gavin, "The Nelder-Mead Algorithm in Two Dimensions," *Department of Civil and Environmental Engineering*, Duke University, 2016.

[Freund-14] R. M. Freund, "Penalty and Barrier Methods for Constrained Optimization," Massachussetts Institute of Techology, 2014.

Index

C

Convergence 59, 60

D

Design of Experiments (DOE) ix, 1, 7, 73, 75
- CCD ix, 25, 26, 30, 55, 71, 75
  - Axial Distance 24, 25
  - Axial Points 24, 25, 27
  - Center Point 24, 27
  - Face-centered vii, ix, 25, 26, 33, 37, 38, 42, 48, 55, 63, 67, 68, 71
  - Rotatableix, 24, 25, 26, 27, 33, 37, 38, 39, 43, 48, 56, 63, 67, 68, 71
  - Spherical 25, 27
- Effect Sparsity 10, 11, 13
- Replicate 9, 16
- Screening Experiment ix, xi, 3, 8, 9, 12, 13, 18, 21, 23, 26, 30, 71
- Factorial 8, 9, 11, 23, 75
  - Fractional 11, 13, 24
    - Alias 11
    - Defining Relation 11
    - Generator 4, 11, 13, 51, 75
    - Resolution 12, 13, 23, 27
- Trial 8, 9, 11, 23
- Unreplicated 9, 10, 21
  - Lenth's Method 10, 16, 17, 18, 21, 75
    - Critical Value 10, 18
    - Cutoff Value 10
    - PSE 10, 17, 18

F

Factor
- Controllabe 5, 6, 21
- Effect 8, 9, 10, 11, 12, 13, 16, 17, 18, 21, 23, 26, 55, 71, 73
  - Active 10, 18, 21, 26, 71
  - Negligible 10, 11, 16, 18, 21
  - Normal Plot 10
- Interaction 8, 9, 10, 11, 13, 16, 18, 21, 23, 71
- Levels 1, 8, 9, 11, 12, 13, 23, 25, 29, 31, 33, 43, 48, 57
- Uncontrollabe ix, 5, 6, 12, 21, 71

Flight Time ix, 3, 12, 14, 15, 16, 21, 26, 30, 33, 43, 54, 56, 62, 64, 67, 69, 71, 72

I

IBIS 6, 75

M

Master-Input Slave-Output (MISO) 50, 57, 63, 67, 68, 72
Master-Output Slave-Input (MOSI) 50, 55, 56, 57, 63, 67, 68, 72
Matlab
- FMINSEARCH 61

N

Noise 9, 15, 32, 58

O

Operating Conditions ix, 6, 21, 27, 71
Optimization ix, 1, 4, 57, 58, 62, 63, 67, 68, 71, 73
- Direct Search 57, 58, 73
  - Differential Evolution 57
  - Genetic Algorithms 57, 73
  - Nelder-Mead vii, ix, xi, 57, 58, 59, 60, 61, 63, 68, 71, 76
  - Simplex 58, 59, 60, 61, 76
  - Transformations 58
    - Contraction 58, 60
    - Expansion 58, 59, 60
    - Reflection 58, 59
    - Shrinkage 58, 60
  - Simulated Annealing 57
- Gradient-Based 57, 73
  - Augmented Lagrangian 57
  - Interior Point Method 57
  - Sequential Programming 57
- Objective Function 58, 59, 60, 61, 62, 63, 67
- Penalty Function ix, 60, 61, 63, 68, 71

R

Regression 23, 26, 27, 28, 30, 31, 32, 33, 36, 37, 38, 43, 47, 49, 55, 56, 63, 64, 67, 69, 72, 73, 76
- Coefficients 23, 30, 32, 33, 36, 38, 55, 62
- Model Fit ix, 31, 37, 55, 71
  - Actual by Predicted plot 31, 32, 33, 36, 37, 39, 42
  - F-test 32

P-value 31, 32
RMSE 31, 32, 37, 38
R-squared 31, 32, 37, 38
R-squared(adjusted) 32, 37, 38
Validation x, 1, 43, 55, 57, 68, 71, 72
Contout Plot 43, 48
Verification 48

S

Serial Peripheral Interface (SPI) vii, ix, xi, 50, 51, 53, 54, 56, 57, 62, 68, 72, 76
Hold Time 51, 54
READ 53, 54, 55, 69, 72
Setup Time 51, 53
WRITE 51, 52, 53, 68, 72
SPICE vii, ix, x, 1, 2, 4, 21, 64, 68, 72
Substitute Model 5
Surrogate Models ix, 1, 5, 57, 71, 73

T

Threshold Region 15
Threshold Voltage 14, 15
Timing Scheme
Common-Clock 50, 51, 53
Source Synchronous 50, 51